Joint Mitigation of Nonlinear RF and Baseband Distortions in Wideband Direct-Conversion Receivers

Published in
IEEE Transactions on Microwave Theory and Techniques

DOI
10.1109/TMTT.2013.2292603

Joint Mitigation of Nonlinear RF and Baseband Distortions in Wideband Direct-Conversion Receivers

Michael Grimm, Markus Allén, *Student Member, IEEE,* Jaakko Marttila, *Student Member, IEEE,* Mikko Valkama, *Member, IEEE,* and Reiner Thomä, *Fellow, IEEE*

***Abstract*—Software-defined radio technology is experiencing more and more attention in modern communication and radar systems. The main practical challenge in deploying such technology is related to achieving sufficient linearity and spurious-free dynamic range in the RF front-end, especially in low-cost mass-product devices. This paper focuses on the analysis and digital mitigation of nonlinear distortion in software-defined radio devices, building on wideband multicarrier/multiradio direct-conversion receiver principle where a wide collection of radio frequencies is I/Q down-converted as a whole. A complete behavioral model for the total nonlinear distortion of the whole receiver chain is first derived, taking into account the third-order nonlinear distortion effects in all individual components, namely RF low-noise amplifier, I/Q mixer and baseband I/Q amplifiers. Stemming from this modeling, adaptive digital feed-forward linearization structure is then developed, to efficiently mitigate the joint nonlinear distortion of the whole receiver. The effectiveness of this approach is verified through extensive simulations and actual RF system measurements with a commercially available software defined radio platform, which clearly outperforms the existing state-of-the-art methods that do not jointly consider RF and baseband nonlinearities.**

***Index Terms*—Cognitive radio, software-defined radio, adaptive signal processing, linearization techniques, nonlinear distortion, interference cancellation, intermodulation distortion**

I. Introduction

The commercial availability of various software-defined radio (SDR) platforms has provided an easy way for experimental radio system research with a highly flexible RF interface. This plays an important role in communications and passive radar applications. Multiradio basestation transceivers in mobile cellular radio systems, with capability of simultaneous transmission and reception at multiple cellular bands and access technologies, form a good example of potential SDR deployment scenarios. In this kind of flexible RF spectrum use, obtaining sufficient linearity and spurious-free dynamic range (SFDR) is one of the biggest challenges [1], especially if one wideband RF chain is deployed, instead of multiple parallel RF chains. Similar challenges are faced in wideband cognitive radio (CR) sensing receivers, as discussed, e.g., in [2] when trying to extract wideband instantaneous radio environment knowledge.

This paper focuses on nonlinear distortion and SFDR challenges in wideband multicarrier/multiradio direct-conversion receivers (DCRs) where a wide collection of radio frequencies is in-phase/quadrature (I/Q) down-converted as a whole. In contrast to the *transmitter* side, the perspective on nonlinear distortion at *receiver* side is fundamentally different. In transmitters, especially when simultaneously transmitting multiple carriers of a single or possibly even multiple radio access technologies through a single power amplifier (PA), there are big challenges with obtaining sufficient linearity [3]. In wideband multiradio receivers, however, nonlinear distortion problems are even more challenging due to the presence of multiple unknown signals, with different power levels and dynamics due to the specific propagation conditions. As the dynamic range within the overall down-converted frequency range can be in the order of 60–100 dB [1], [2], such wideband receivers are extremely prone to any imperfections in the RF analog components. In general, essential receiver RF impairments include DC offsets due to self-mixing, oscillator phase noise, I/Q imbalance, and nonlinear distortions [1]. In particular, I/Q imbalance and nonlinear distortion effects of the receiver components can severely degrade the demodulation performance at weak signal bands, and also heavily affect the reliability of spectrum monitoring or sensing in CR [2], [4]–[8]. In multiradio receivers, the most challenging scenarios arise when the same wideband RF chain is simultaneously receiving multiple GSM, UMTS/WCDMA and LTE carriers, and some of them are close to the maximum allowed blocking signal level whereas some others are close to the receiver sensitivity level. In these kind of scenarios, the intermodulation distortion (IMD) of strong blocking carriers can easily mask the weaker signals, thus requiring extreme linearity from the receiver. Similar challenges exist in wideband CR sensing receivers, where some of the primary user signals can be close to the thermal noise floor, but should still be identified in the presence of other strong co-existing signals. Additionally,

Manuscript received July 8, 2013; revised November 8, 2013; accepted November 15, 2013. This work was supported by the Finnish Funding Agency for Technology and Innovation (Tekes) under the project "Enabling Methods for Dynamic Spectrum Access and Cognitive Radio," the Academy of Finland under the project 251138 "Digitally-Enhanced RF for Cognitive Radio Devices," Austrian Competence Center in Mechatronics (ACCM), TUT Graduate School, Nokia Foundation, and the International Graduate School on Mobile Communications supported by the German Research Foundation (DFG GRK1487).

M. Grimm and R. Thomä are with the Electronic Measurement Research Lab, Institute for Information Technology, Ilmenau University of Technology, 98684 Ilmenau, Germany (e-mail: michael.grimm@tu-ilmenau.de, reiner.thomae@tu-ilmenau.de).

M. Allén, J. Marttila, and Mikko Valkama are with the Department of Electronics and Communications Engineering, Tampere University of Technology, P.O. Box 692, FI-33101 Tampere, Finland (e-mail: markus.allen@tut.fi, jaakko.marttila@tut.fi, mikko.e.valkama@tut.fi).

strong nonlinear distortion can cause false alarms in spectrum sensing when a vacant channel contains the distortion and is falsely interpreted as being occupied by a primary user [7]. Compared to conventional receiver architectures with multiple intermediate frequency (IF) stages, most of the selectivity in DCR front-ends is implemented at the baseband (BB) or only in digital domain in favor of flexibility and operation over a wide bandwidth. Therefore, linearity and dynamic range requirements are extremely stringent.

In this paper, we address the modeling and digital mitigation of nonlinear distortion of all the essential RF analog components of a wideband DCR. In the existing literature, mitigating receiver nonlinear distortion by means of BB digital signal processing has been proposed in [9], [10], and subsequently followed in [7], [11]–[15], among others. Furthermore, specific even-order distortion mitigation in classical narrowband DCR context is addressed in [16]. In all these works, specific reference models of considered nonlinear components are applied, either in analog or digital domain, to regenerate considered distortion products and to subtract them from the received signal. Previous works [7], [9], [10], [12], [13], [17] all focus on specific receiver component only, namely RF low-noise amplifier (LNA), BB amplifiers or analog-to-digital converter (ADC), whereas [14] provides specific application of distortion mitigation to interference scenarios in GSM downlink. Furthermore, customized analog receiver designs were proposed in [11] and [12] to overcome specific limitations of entirely digital processing based approaches.

According to the best knowledge of the authors, however, modeling and mitigation of the nonlinearities induced by a complete DCR chain, including RF LNA, I/Q mixer and BB I/Q amplifiers, as well as their interaction with mixer I/Q imbalance is missing from the existing state-of-the-art literature. As all these components behave in a nonlinear manner in practice, understanding and being able to mitigate the joint nonlinear distortion effects are seen critical and therefore addressed in this paper. Contrary to conventional spectral regrowth around the distortion-producing signal, distortion products in DCRs are created by RF and BB receiver components and may fall within the BB bandwidth. Thus, we first derive the complete behavioral model for the total nonlinear distortion, which takes into account the third-order nonlinear distortion of the RF LNA, I/Q imbalance of the I/Q mixer, and third-order nonlinear distortion of the mixer and BB amplifiers. Individual component modeling is kept at third-order level since third-order distortion is the most dominant one in practice, and the presentation and notations are also simplified. Notice, however, that from the total receiver distortion modeling perspective, up to ninth-order distortion modeling is supported by joint modeling of RF and BB distortion. Stemming from this modeling, efficient DSP-based linearization structure, together with practical adaptive filtering based learning algorithms, are then developed. All the signal processing developments are non-data-aided (blind), as in general received signals are unknown due to unknown modulating data and unknown propagation conditions. Thus, the developed linearization can be carried out in the very first stages of the receiver digital front-end, prior to any modulation- or system-specific processing and carrier-/timing synchronization. This is a substantial practical benefit, compared to data-aided approaches, since heavy nonlinear distortion can also easily hinder the operation of, e.g., synchronization algorithms. Finally, extensive computer simulation results, as well as actual RF system measurements with commercial SDR platform, namely Universal Software Radio Peripheral (USRP) [18], are provided. Based on the obtained results, the developed linearization scheme clearly outperforms the existing reference methods, which can only suppress the effects of individual receiver components. Thus, the developed linearization solution can be seen as one key enabling technique towards practical deployment of SDR technology with digitally-enhanced wideband RF front-ends.

The outline of the remainder of the paper is as follows. In the following Section II, nonlinear distortion effects and mirror-frequency interference created in the DCR chain are discussed and modeled in detail, first component-wise and then accumulated into a total composite model. Based on that joint model, Section III then develops the proposed digital mitigation architecture and associated parameter learning algorithms. Simulation and RF measurement results are presented and analyzed in Section IV, whereas Section V gives further discussions, result analysis, and outlook on future work. Finally, conclusions are drawn in Section VI.

II. Nonlinear Distortion Analysis in Wideband Direct-Conversion Receivers

This section gives a detailed description of nonlinearities occurring in DCRs and a derivation of a complete mathematical model, combining RF and BB stage nonlinearities.

A. Receiver Architecture and Signal Scenario of Interest

DCRs have become more popular due to their inherent advantages over superheterodyne receivers [1], [19]. The DCR architecture is compact since the frequency translation from RF to BB is performed by a single mixing stage. The direct down-conversion allows signal amplification and filtering at BB, therefore, decreasing power consumption and simplifying image rejection. Altogether, these benefits ease the implementation of the whole receiver as a monolithic integrated circuit and decrease its manufacturing cost. However, DCRs suffer from the RF and BB impairments, such as I/Q imbalance and nonlinear distortion, as discussed in Section I.

Fig. 1 depicts a basic block diagram of a DCR with quadrature down-conversion, which generally consists of analog RF, mixer, analog BB, and digital post-processing stages. In practice, analog RF and BB stages suffer from unavoidable nonlinear behavior. Distortions that are created at the RF amplifier are typically dominating distortions created at the BB stages. However, they depend on the deployed components. In addition, the RF filtering provides very low selectivity. Thus, strong out-of-band signals can easily enter the front-end amplification and mixing stages. Beside receiver nonlinearity, I/Q imbalance of the mixer and the BB I/Q branches cause distorting mirror signal components that may interfere with other useful signals.

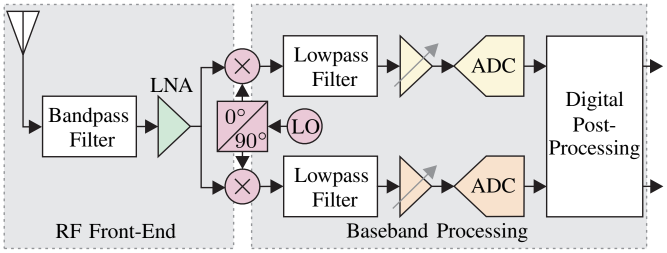

Fig. 1. Conceptual direct-conversion receiver block diagram. In wideband receiver scenario, multiple carriers and possibly also radio access technologies are received simultaneously, and selectivity filtering is implemented in the digital parts.

The most challenging case in deploying the direct-conversion radio architecture is the wideband multicarrier/multiradio scenario where the down-converted signal contains multiple carriers of multiple co-existing radio access technologies, throughout the whole receiver chain through the A/D interface. This kind of scenario leads to high dynamic range signal configurations with weak and strong signals simultaneously present. It is then likely that nonlinear distortions caused by strong signals fall on top of weak desired signals or leak into free frequency bands in case of CR sensing receiver. In CR context, free frequency bands are typically called white spaces [4]. Receiver distortion may mask a white space so that spectrum sensing algorithms falsely consider it to be occupied, which causes the CR to be less efficient from the spectrum exploitation point of view. Since multiple signals from different sources may, in general, arrive at the antenna input, mitigation of distortions created in the receiver becomes more challenging than in a transmitter, where the signal sources are well-known inside the device. Therefore, proper modeling of DCRs is essential to clean the whole BB from all distortions stemming from the strong input signals.

B. RF Nonlinearities

In this paper, BB equivalent signal modeling is used as it is notationally convenient and widely adopted convention [20]. The received bandpass signal $x_{\mathrm{RF}}(t)$ can be presented as

$$x_{\mathrm{RF}}(t) = 2\,\mathrm{Re}[x(t)e^{j\omega_{\mathrm{c}}t}] = x(t)e^{j\omega_{\mathrm{c}}t} + x^*(t)e^{-j\omega_{\mathrm{c}}t}, \quad (1)$$

where ω_{c} is the angular center frequency of the total RF signal to be down-converted and $x(t)$ is the corresponding BB equivalent signal of $x_{\mathrm{RF}}(t)$ ($(\cdot)^*$ denotes complex conjugate). Notice that in this notation, in case of wideband multicarrier down-conversion, the BB equivalent signal $x(t)$ contains all individual carrier waveforms at different complex IFs. Furthermore, $x(t)$ is defined as

$$x(t) = A(t)e^{j\phi(t)} = x_{\mathrm{I}}(t) + jx_{\mathrm{Q}}(t), \quad (2)$$

where $A(t)$ and $\phi(t)$ are the total envelope and phase of the overall down-converted RF signal $x(t)$, whereas $x_{\mathrm{I}}(t)$ and $x_{\mathrm{Q}}(t)$ denote the corresponding composite I and Q signals, respectively. The signal model (2) provides a starting point for modeling RF and BB nonlinearities of DCRs. This leads to the structure shown in Fig. 2, where also simplified BB equivalent spectra are illustrated, with only one active carrier for visualization purposes. Next, more detailed modeling of the RF LNA nonlinearities is addressed.

From the actual RF signal perspective, the RF nonlinearities can be modeled using a generalized Hammerstein model

$$y_{\mathrm{RF}}(t) = b_1(t) * x_{\mathrm{RF}}(t) + b_2(t) * x_{\mathrm{RF}}^2(t) + \ldots, \quad (3)$$

where $b_1(t), b_2(t), b_3(t), \ldots$ are impulse responses for each nonlinearity order taking memory effects into account [21]. In practice, (3) models the nonlinear behavior of the LNA in the RF stage. Using this notation, the input of the LNA in Fig. 1 is $x_{\mathrm{RF}}(t)$ and the output is $y_{\mathrm{RF}}(t)$. While (3) provides the general model, it is possible to simplify it and still capture the most essential behavior of the DCR. Even-order RF nonlinearities produce new frequency components, which are in most cases far away from ω_{c} and thus most likely to be filtered out. For example, an equation obtained from (1) and (3) for the second-order nonlinearity

$$x_{\mathrm{RF}}^2(t) = 2x(t)x^*(t) + x^2(t)e^{j2\omega_{\mathrm{c}}t} + [x^*(t)]^2e^{-j2\omega_{\mathrm{c}}t} \quad (4)$$

illustrates the new frequencies appearing around $\pm 2\omega_{\mathrm{c}}$ and DC (zero frequency), but no IMD components are created within the interesting RF bandwidth around ω_{c}. However, IMD contained in $x_{\mathrm{RF}}(t)$ cannot be seen directly from (4). These even-order RF IMD components are usually not harmful, except if the RF front-end is extremely wideband and $x_{\mathrm{RF}}(t)$ consists of several strong signals, which are far away from each other [2]. Even in this case, the even-order effects are not significant when proper circuit design methodologies providing high second-order intercept points are employed [2], [22]. In addition, the even-order nonlinearities induce spectral content around DC, such as $2x(t)x^*(t) = 2A^2(t)$ in (4), but it can be removed effectively with AC-coupling or filtering [2], [23]. Odd-order nonlinearities are, however, more critical since they cause new frequency components near ω_{c}, i.e., within the total frequency band of interest. In practice, the third-order nonlinearity is usually the strongest and the only one among the RF nonlinearity orders that appears clearly above the noise level. Therefore, a simplified RF nonlinearity model

$$y'_{\mathrm{RF}}(t) = a_1x_{\mathrm{RF}}(t) + a_2x_{\mathrm{RF}}^3(t) \quad (5)$$

is considered here, in which memory effects are omitted for notational simplicity and hence scalar coefficients a_1 and a_2, instead of filters $b_1(t)$ and $b_3(t)$, are used. This leads to the widely-used memoryless polynomial model [10], [24]. The lack of memory simplifies the notation in this analysis so that the most essential interpretations of the nonlinearity phenomenon can be made more easily. The memory effects are then taken into account later in the next section when impairment mitigation is discussed. The coefficients a_1 and a_2 are chosen to be complex in order to model AM/PM distortion of the LNA [24].

To further analyze the new spectral content by the third-order RF nonlinearity, the latter term of (5) can be written as

$$\begin{aligned} a_2x_{\mathrm{RF}}^3(t) &= a_2\{x(t)e^{j\omega_{\mathrm{c}}t} + x^*(t)e^{-j\omega_{\mathrm{c}}t}\}^3 \\ &= a_2\{x^3(t)e^{j3\omega_{\mathrm{c}}t} + [x^*(t)]^3e^{-j3\omega_{\mathrm{c}}t} \\ &\quad + 3x^2(t)x^*(t)e^{j\omega_{\mathrm{c}}t} + 3x(t)[x^*(t)]^2e^{-j\omega_{\mathrm{c}}t}\}. \end{aligned} \quad (6)$$

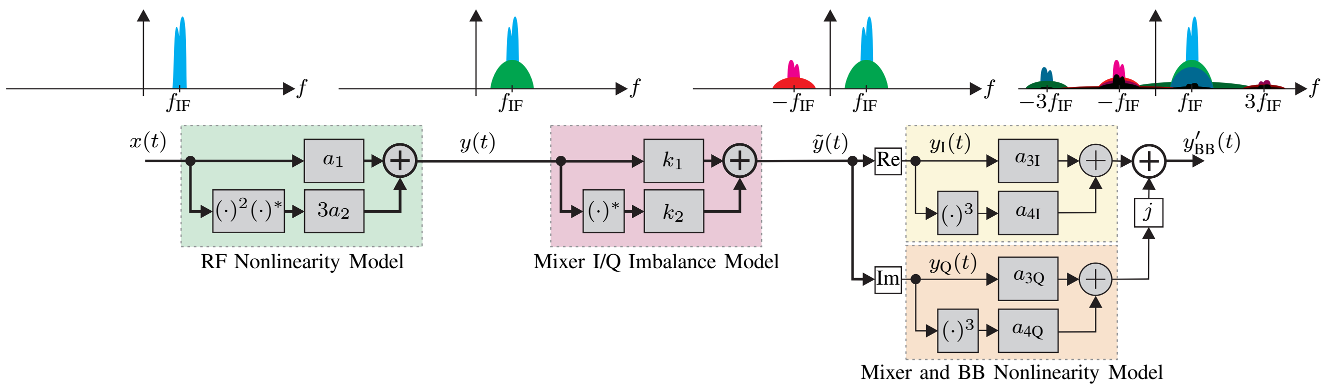

Fig. 2. Cascaded model considering third-order RF and BB nonlinearities in the presence of mixer and BB I/Q imbalance. Due to the generality of the nonlinearity models, they also take mixer nonlinearities into account. The spectrum illustrations are sketched for BB equivalent signals matching to the mathematical modeling in the paper, and only a single carrier is shown for visualization purposes.

From (6) it is apparent that there is only one term that causes new frequency content around ω_{c}, i.e., $3a_2x^2(t)x^*(t)e^{j\omega_{\text{c}}t}$. The effective RF nonlinearity contribution comes from this particular term since it is shifted to the BB in the I/Q down-conversion stage whereas the other three terms in (6) do not hit the BB and are hence filtered out. Therefore, the essential BB equivalent form of (5) after the BB filtering becomes

$$\begin{aligned} y(t) &= y_{\text{I}}(t) + jy_{\text{Q}}(t) \\ &= a_1x(t) + 3a_2x^2(t)x^*(t) \\ &= a_1x(t) + 3a_2A^2(t)x(t) \\ &= a_1x(t) + 3a_2z(t). \end{aligned} \tag{7}$$

The second-last form of (7) is stemming from the fact that $x(t)x^*(t) = |x(t)|^2 = A^2(t)$. An auxiliary variable $z(t)$ is introduced here to denote the RF distortion contribution and make some of the further equations easier to interpret. The real and imaginary parts of $y(t)$ can be written as

$$\begin{aligned} y_{\text{I}}(t) &= a_1x_{\text{I}}(t) + 3a_2[x_{\text{I}}^3(t) + x_{\text{I}}(t)x_{\text{Q}}^2(t)] \\ &= a_1x_{\text{I}}(t) + 3a_2A^2(t)x_{\text{I}}(t) \\ &= a_1x_{\text{I}}(t) + 3a_2z_{\text{I}}(t), \end{aligned} \tag{8a}$$

$$\begin{aligned} y_{\text{Q}}(t) &= a_1x_{\text{Q}}(t) + 3a_2[x_{\text{I}}^2(t)x_{\text{Q}}(t) + x_{\text{Q}}^3(t)] \\ &= a_1x_{\text{Q}}(t) + 3a_2A^2(t)x_{\text{Q}}(t) \\ &= a_1x_{\text{Q}}(t) + 3a_2z_{\text{Q}}(t). \end{aligned} \tag{8b}$$

It is worth noticing that the term $3a_2A^2(t)x(t)$ only causes distortion around the center frequency of $x(t)$. However, the bandwidth of the distortion is wider than of $x(t)$, because of the multiplication with the squared envelope $A^2(t)$.

After the LNA, the signal goes through a wideband I/Q down-conversion stage as depicted in Fig. 1. In practice, an I/Q mixer cannot provide exactly 90° phase shift as desired but sustains a phase mismatch of ϕ_{m} (rad). Additionally, the I/Q mixer suffers from a relative amplitude mismatch g_{m} between the I and Q branches. These mismatches cause I/Q imbalance, which is seen as mirroring of frequency content of $y(t)$. More detailed information about I/Q imbalance can be found in [25], [26], and references therein. The I/Q imbalance of the down-conversion stage is here modeled as

$$\tilde{y}(t) = k_1y(t) + k_2y^*(t), \tag{9}$$

where the complex mismatch coefficients are

$$k_1 = \left(1 + g_{\text{m}}e^{-j\phi_{\text{m}}}\right)/2, \tag{10a}$$

$$k_2 = \left(1 - g_{\text{m}}e^{j\phi_{\text{m}}}\right)/2. \tag{10b}$$

With perfect I/Q balance, $g_{\text{m}} = 1$, $\phi_{\text{m}} = 0$ and hence $k_1 = 1$, $k_2 = 0$. The RF-distorted signal with I/Q imbalance $\tilde{y}(t) = \tilde{y}_{\text{I}}(t) + j\tilde{y}_{\text{Q}}(t)$ can now be expressed as

$$\tilde{y}_{\text{I}}(t) = y_{\text{I}}(t), \tag{11a}$$

$$\tilde{y}_{\text{Q}}(t) = g_{\text{m}}\cos(\phi_{\text{m}})y_{\text{Q}}(t) - g_{\text{m}}\sin(\phi_{\text{m}})y_{\text{I}}(t). \tag{11b}$$

The results presented in (8) and (11) are important in a sense that $\tilde{y}(t)$ is the signal distorted by both RF nonlinearities and mixer I/Q imbalance, and hence describes their joint impact. More specifically, the signal at this point contains the intermodulation distortion created by the RF LNA and its mirror image symmetrically around zero-frequency, as well as the actual mirror image of the ideal signal. These are illustrated in Fig. 2. Next, the I and Q signals become further distorted through mixer and baseband nonlinearities. This is elaborated further in the following subsection.

C. Mixer and Baseband Nonlinearities

BB nonlinearity modeling differs from RF nonlinearities in such a way that in the BB there are physically separate I and Q branches in which the nonlinearities occur independently. In general, for the distorted BB signal $y_{\text{BB}}(t) = y_{\text{I,BB}}(t) + jy_{\text{Q,BB}}(t)$, the generalized Hammerstein model is

$$y_{\text{I,BB}}(t) = c_{1\text{I}}(t) * \tilde{y}_{\text{I}}(t) + c_{2\text{I}}(t) * \tilde{y}_{\text{I}}^2(t) + \ldots, \tag{12a}$$

$$y_{\text{Q,BB}}(t) = c_{1\text{Q}}(t) * \tilde{y}_{\text{Q}}(t) + c_{2\text{Q}}(t) * \tilde{y}_{\text{Q}}^2(t) + \ldots, \tag{12b}$$

where $c_{1\text{I}}(t), c_{2\text{I}}(t), c_{3\text{I}}(t), \ldots$ and $c_{1\text{Q}}(t), c_{2\text{Q}}(t), c_{3\text{Q}}(t), \ldots$ are impulse responses for each nonlinearity order in the I and Q branches. This model basically takes into account all the nonlinearities of BB components shown in Fig. 1, specifically amplifiers and ADCs, and also mixers since the I/Q mixer outputs are already at down-converted frequencies. In the following, the term “BB nonlinearities” is used to cover these as a whole. There are different impulse responses for I and Q polynomials, because nonlinearities themselves can be different in the I and Q branches since those contain physically separate components in practice. Furthermore, BB circuit components in the I and Q branches typically have slightly different gain characteristics, which introduce I/Q imbalance. In general, this I/Q imbalance is frequency-dependent as discussed in [25], [26].

Similar to the RF nonlinearities, simplifications to the BB model are justifiable. Only the third-order BB nonlinearity is considered here as it describes the most significant distortions. Even-order distortions are very weak due to efficient circuit design solutions such as differential signaling [27]. In typical DCRs, signaling behind the LNA is performed symmetrically, i.e., by using two signals that are ideally 180° out of phase. The differential voltage can be written as $V_{\text{diff}} = V_+ - V_-$. By writing down (12a) or (12b) for V_+ and V_- and computing the differential voltage V_{diff}, it can be shown that even-order terms cancel out, whereas odd-order terms increase by factor two [27]. However, even-order cancellation by differential signaling requires a symmetrical layout and matched amplifiers to ensure perfect balance among the signals. The minor importance of even-order distortions is also presented by the measurements in Section IV. Furthermore, higher odd-order distortions are typically masked by noise in practice. Therefore, the simplified model becomes

$$y'_{\text{I,BB}}(t) = a_{3\text{I}}\tilde{y}_{\text{I}}(t) + a_{4\text{I}}\tilde{y}_{\text{I}}^3(t), \tag{13a}$$

$$y'_{\text{Q,BB}}(t) = a_{3\text{Q}}\tilde{y}_{\text{Q}}(t) + a_{4\text{Q}}\tilde{y}_{\text{Q}}^3(t), \tag{13b}$$

where the real-valued scalar coefficients $a_{3\text{I}}$, $a_{3\text{Q}}$, $a_{4\text{I}}$, and $a_{4\text{Q}}$ are used, instead of the filters $c_{1\text{I}}(t)$, $c_{1\text{Q}}(t)$, $c_{3\text{I}}(t)$, and $c_{3\text{Q}}(t)$. This means that the memory effects are omitted in this analysis phase similar to the RF nonlinearities in (5). However, the forthcoming digital mitigation signal processing in Section III is devised such that also frequency-dependent effects can be tackled. The obtained complete nonlinearity model, combining RF and BB nonlinearities with I/Q imbalances, is visualized with a block diagram in Fig. 2.

D. Model Interactions and Interpretations

First, assuming perfectly balanced I/Q mixer, i.e. $\tilde{y}(t) = y(t)$, Equations (13a) and (13b) can be further modified by substituting $y_{\text{I}}(t)$ and $y_{\text{Q}}(t)$ from (8a) and (8b) so that

$$\begin{aligned}
y'_{\text{I,BB}}(t) &= a_{3\text{I}}a_1x_{\text{I}}(t) + 3a_{3\text{I}}a_2z_{\text{I}}(t) \\
&\quad + a_{4\text{I}}a_1^3x_{\text{I}}^3(t) + 9a_{4\text{I}}a_1^2a_2x_{\text{I}}^2(t)z_{\text{I}}(t) \\
&\quad + 27a_{4\text{I}}a_1a_2^2x_{\text{I}}(t)z_{\text{I}}^2(t) + 27a_{4\text{I}}a_2^3z_{\text{I}}^3(t) \\
&= a_{3\text{I}}[a_1 + 3a_2A^2(t)]x_{\text{I}}(t) \\
&\quad + a_{4\text{I}}[a_1^3 + 9a_1^2a_2A^2(t) \\
&\quad + 27a_1a_2^2A^4(t) + 27a_2^3A^6(t)]x_{\text{I}}^3(t),
\end{aligned} \tag{14a}$$

$$\begin{aligned}
y'_{\text{Q,BB}}(t) &= a_{3\text{Q}}a_1x_{\text{Q}}(t) + 3a_{3\text{Q}}a_2z_{\text{Q}}(t) \\
&\quad + a_{4\text{Q}}a_1^3x_{\text{Q}}^3(t) + 9a_{4\text{Q}}a_1^2a_2x_{\text{Q}}^2(t)z_{\text{Q}}(t) \\
&\quad + 27a_{4\text{Q}}a_1a_2^2x_{\text{Q}}(t)z_{\text{Q}}^2(t) + 27a_{4\text{Q}}a_2^3z_{\text{Q}}^3(t) \\
&= a_{3\text{Q}}[a_1 + 3a_2A^2(t)]x_{\text{Q}}(t) \\
&\quad + a_{4\text{Q}}[a_1^3 + 9a_1^2a_2A^2(t) \\
&\quad + 27a_1a_2^2A^4(t) + 27a_2^3A^6(t)]x_{\text{Q}}^3(t).
\end{aligned} \tag{14b}$$

The expressions in (14) clearly show the interaction between the RF and BB stages. In other words, the BB nonlinearities are affecting the original signal as well as the RF distortion components and, therefore, more elaborate and complicated total intermodulation profile is created. It is noteworthy that some of the new frequency components would not appear, if RF and BB nonlinearities were modeled independently, i.e., in (12a) and (12b) there would be $x_{\text{I}}(t)$ and $x_{\text{Q}}(t)$ instead of $\tilde{y}_{\text{I}}(t)$ and $\tilde{y}_{\text{Q}}(t)$. It is noteworthy that (14a) and (14b) can be also written as

$$\begin{aligned}
y'_{\text{I,BB}}(t) &= 27a_{4\text{I}}a_2^3x_{\text{I}}^9(t) + 81a_{4\text{I}}a_2^3x_{\text{I}}^7(t)x_{\text{Q}}^2(t) \\
&\quad + 27a_{4\text{I}}a_1a_2^2x_{\text{I}}^7(t) + 81a_{4\text{I}}a_2^3x_{\text{I}}^5x_{\text{Q}}^4 \\
&\quad + 54a_{4\text{I}}a_1a_2^2x_{\text{I}}^5(t)x_{\text{Q}}^2(t) + 9a_{4\text{I}}a_1^2a_2x_{\text{I}}^5(t) \\
&\quad + 27a_{4\text{I}}a_2^3x_{\text{I}}^3(t)x_{\text{Q}}^6(t) + 27a_{4\text{I}}a_1a_2^2x_{\text{I}}^3(t)x_{\text{Q}}^4(t) \\
&\quad + 9a_{4\text{I}}a_1^2a_2x_{\text{I}}^3(t)x_{\text{Q}}^2(t) + (a_{4\text{I}}a_1^3 + 3a_{3\text{I}}a_2)x_{\text{I}}^3(t) \\
&\quad + a_{3\text{I}}a_23x_{\text{I}}(t)x_{\text{Q}}^2(t) + a_{3\text{I}}a_1x_{\text{I}}(t),
\end{aligned} \tag{15a}$$

$$\begin{aligned}
y'_{\text{Q,BB}}(t) &= 27a_{4\text{Q}}a_2^3x_{\text{Q}}^9(t) + 81a_{4\text{Q}}a_2^3x_{\text{I}}^2(t)x_{\text{Q}}^7(t) \\
&\quad + 27a_{4\text{Q}}a_1a_2^2x_{\text{Q}}^7(t) + 81a_{4\text{Q}}a_2^3x_{\text{I}}^4x_{\text{Q}}^5 \\
&\quad + 54a_{4\text{Q}}a_1a_2^2x_{\text{I}}^2(t)x_{\text{Q}}^5(t) + 9a_{4\text{Q}}a_1^2a_2x_{\text{Q}}^5(t) \\
&\quad + 27a_{4\text{Q}}a_2^3x_{\text{I}}^6(t)x_{\text{Q}}^3(t) + 27a_{4\text{Q}}a_1a_2^2x_{\text{I}}^4(t)x_{\text{Q}}^3(t) \\
&\quad + 9a_{4\text{Q}}a_1^2a_2x_{\text{I}}^2(t)x_{\text{Q}}^3(t) \\
&\quad + (a_{4\text{Q}}a_1^3 + 3a_{3\text{Q}}a_2)x_{\text{Q}}^3(t) + a_{3\text{Q}}a_1x_{\text{Q}}(t) \\
&\quad + 3a_{3\text{Q}}a_2x_{\text{I}}^2(t)x_{\text{Q}}(t).
\end{aligned} \tag{15b}$$

These equations are obtained using only $x_{\text{I}}(t)$ and $x_{\text{Q}}(t)$ instead of the envelope $A(t)$. From (15a) and (15b) it can be seen directly that the third-order nonlinearities in the RF and BB cause distortion components of up to ninth order. Due to the space limitations and extensive amount of terms (46 instead of 13), the I/Q imbalanced version of (15) is omitted here. However, the I/Q imbalance effects are considered in the next paragraph with the aid of complex equations, which contain the same information in more concise form.

The complex representation of (13a) and (13b), i.e., $y'_{\text{BB}}(t) = y'_{\text{I,BB}}(t) + jy'_{\text{Q,BB}}(t)$ is useful from the analysis point of view, because it reveals how the distortion components are spectrally distributed in relation to the original signal. In the general form with the I/Q imbalance included, the complete distorted signal is as written in (16) (next page). As $y(t)$ comprises the original signal and its RF distortion components, both have also mirror components, i.e. $y^*(t)$, if mixer and/or BB I/Q imbalance occurs. In addition, the BB nonlinearities cause third-order terms, $y^3(t)$ and $[y^*(t)]^3$, which contribute to the harmonics and IMD of the original down-converted signal and associated RF distortion components. There is also another pair of third-order terms stemming from the BB nonlinearities, namely $y^2(t)y^*(t)$ and $y(t)[y^*(t)]^2$. These represent further spreading around the already existing frequency components similarly as is discussed in the previous subsection for the RF distortions. It is noteworthy that the mixer I/Q imbalance has essential impact as it propagates to all aforementioned terms. If perfect I/Q mixer balance ($k_1 = 1, k_2 = 0$) is assumed, the expression in (16) shortens significantly from the coefficients' perspective, but the number of y-terms stays the same. This is seen by writing the signal explicitly as

$$
\begin{aligned}
y'_{\mathrm{BB}}(t) = &\frac{a_{3\mathrm{I}}+a_{3\mathrm{Q}}}{2}y(t)+\frac{a_{3\mathrm{I}}-a_{3\mathrm{Q}}}{2}y^*(t)\\
&+\frac{a_{4\mathrm{I}}-a_{4\mathrm{Q}}}{8}y^3(t)+\frac{a_{4\mathrm{I}}+a_{4\mathrm{Q}}}{8}[y^*(t)]^3\\
&+\frac{3a_{4\mathrm{I}}+3a_{4\mathrm{Q}}}{8}y^2(t)y^*(t)\\
&+\frac{3a_{4\mathrm{I}}-3a_{4\mathrm{Q}}}{8}y(t)[y^*(t)]^2.
\end{aligned}
\tag{17}
$$

This form illustrates well how the BB I/Q imbalance affects the signal in the presence of nonlinearities. Notice that in case of perfect I/Q balance (both the mixer and BB), the number of terms in (17) reduces to three, namely $y(t)$, $[y^*(t)]^3$, and $y^2(t)y^*(t)$.

Table I provides a summary of the terms produced by the cascaded nonlinearity model without any kind of I/Q imbalance. In other words, the tabulated terms stem from $y(t)$, $[y^*(t)]^3$, and $y^2(t)y^*(t)$. The time variable (t) and all coefficients for the terms are omitted from Table I to enhance readability. The first column lists all nine terms using $x(t)$ and $z(t)$. In the second column, the same terms are written using $x(t)$ and its envelope $A(t)$. This form shows very intuitively the spectral contribution of each term separately as $x(t)$ means contributions around the original center frequency whereas $(x^*)^3$ refers to the opposite side of the spectrum with three times the original center frequency and triple the bandwidth. Different powers of $A(t)$ refer to the spreading with respect to the original bandwidth. The last column of Table I indicates the relationships between the complex terms and separate I and Q branch processing. It is noteworthy that each term having separate I and Q processing corresponds to two complex terms. In addition, any I/Q imbalance in the mixer or BB results in another nine terms, which are the complex conjugates of the ones shown in Table I.

TABLE I
ALTERNATIVE FORMS FOR THE TERMS PRODUCED BY THE CASCADED NONLINEARITY MODEL WITHOUT I/Q IMBALANCE

#	$z = x^2x^*$	$A^2 = xx^*$	I/Q Representation
1	x	x	$x_{\mathrm{I}} + jx_{\mathrm{Q}} = x$
2	z	A^2x	$x_{\mathrm{I}}^3 + jx_{\mathrm{Q}}^3 = \frac{1}{4}(x^*)^3 + \frac{3}{4}A^2x$
3	$(x^*)^3$	$(x^*)^3$	
4	x^2z^*	A^4x	$x_{\mathrm{I}}^2z_{\mathrm{I}} + jx_{\mathrm{Q}}^2z_{\mathrm{Q}} = \frac{1}{4}A^2(x^*)^3 + \frac{3}{4}A^4x$
5	$(x^*)^2z^*$	$A^2(x^*)^3$	
6	x^*z^2	A^6x	$x_{\mathrm{I}}z_{\mathrm{I}}^2 + jx_{\mathrm{Q}}z_{\mathrm{Q}}^2 = \frac{1}{4}A^4(x^*)^3 + \frac{3}{4}A^6x$
7	$x^*(z^*)^2$	$A^4(x^*)^3$	
8	z^2z^*	A^8x	$z_{\mathrm{I}}^3 + jz_{\mathrm{Q}}^3 = \frac{1}{4}A^6(x^*)^3 + \frac{3}{4}A^8x$
9	$(z^*)^3$	$A^6(x^*)^3$	

III. PROPOSED MITIGATION ARCHITECTURE FOR CASCADED NONLINEARITY

The digital nonlinearity mitigation approach proposed in this paper bases its foundation on the adaptive interference cancellation concept originally presented in [9], [10]. However, [9] and [10] consider only either RF or BB nonlinearities but not their joint effect, and are thus clearly limited in performance as shown by the nonlinearity analysis in the previous section. This section discusses in detail how the nonlinearity model from the previous section can be exploited for joint distortion mitigation purposes. Additionally, the differences between spectrum sensing and individual IF carrier demodulation scenarios are highlighted from the mitigation structure point of view. First, Subsection A explains the mitigation concept in detail and Subsection B then provides a practically implementable mitigation structure based on that concept.

A. Mitigation Concept

The basic mitigation principle is illustrated in Fig. 3 in case of *spectrum sensing scenario*, where the goal is to eliminate the distortions from the whole reception bandwidth in order to enhance the spectrum sensing [2], [4], [7]. This model is also valid in multicarrier/multiradio basestation receiver that is designed to demodulate all the down-converted carriers simultaneously. After digitalization, the received signal $y'_{\mathrm{BB}}(n)$ goes through a band-splitting stage, which divides the signal into a main path $d(n)$ and a reference path $\hat{x}(n)$. The main path contains the signal after the bandstop filter of the band-splitting stage, i.e., all the signal content except the strongest blocker(s). Correspondingly, the reference path contains only the strongest blocker(s) and regenerates the total nonlinear distortion stemming from them. Finally, the regenerated distortion is subtracted from the main path signal $d(n)$ in order to remove the distortions. In the reference path, the receiver RF and BB

$$
\begin{aligned}
y'_{\mathrm{BB}}(t) = &\left\{\frac{a_{3\mathrm{I}}+a_{3\mathrm{Q}}}{2}k_1+\frac{a_{3\mathrm{I}}-a_{3\mathrm{Q}}}{2}k_2^*\right\}y(t)+\left\{\frac{a_{3\mathrm{I}}+a_{3\mathrm{Q}}}{2}k_2+\frac{a_{3\mathrm{I}}-a_{3\mathrm{Q}}}{2}k_1^*\right\}y^*(t)\\
&+\left\{\frac{a_{4\mathrm{I}}-a_{4\mathrm{Q}}}{8}\left[k_1^3+3k_1(k_2^*)^2\right]+\frac{a_{4\mathrm{I}}+a_{4\mathrm{Q}}}{8}\left[(k_2^*)^3+3k_1^2k_2^*\right]\right\}y^3(t)\\
&+\left\{\frac{a_{4\mathrm{I}}-a_{4\mathrm{Q}}}{8}\left[k_2^3+3(k_1^*)^2k_2\right]+\frac{a_{4\mathrm{I}}+a_{4\mathrm{Q}}}{8}\left[(k_1^*)^3+3k_1^*k_2^2\right]\right\}[y^*(t)]^3\\
&+\left\{\frac{a_{4\mathrm{I}}-a_{4\mathrm{Q}}}{8}3\left[{k_1}^2k_2+|k_2|^2k_2^*+2|k_1|^2k_2^*\right]+\frac{a_{4\mathrm{I}}+a_{4\mathrm{Q}}}{8}3\left[k_1^*(k_2^*)^2+|k_1|^2k_1+2|k_2|^2k_1\right]\right\}y^2(t)y^*(t)\\
&+\left\{\frac{a_{4\mathrm{I}}-a_{4\mathrm{Q}}}{8}3\left[k_1k_2^2+|k_1|^2k_1^*+2|k_2|^2k_1^*\right]+\frac{a_{4\mathrm{I}}+a_{4\mathrm{Q}}}{8}3\left[(k_1^*)^2k_2^*+|k_2|^2k_2+2|k_1|^2k_2\right]\right\}y(t)[y^*(t)]^2
\end{aligned}
\tag{16}
$$

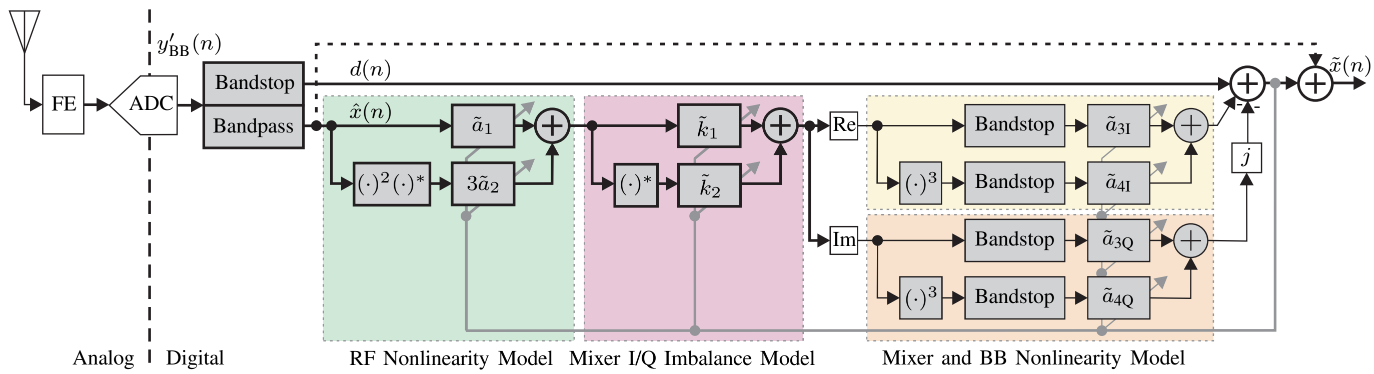

Fig. 3. Principal cascaded adaptive digital mitigation structure for cascaded RF and BB nonlinearities with mixer and BB I/Q imbalance.

nonlinearities and also I/Q imbalance are modeled as discussed in Section II in order to create the needed distortion estimates. The coefficients $\tilde{a}_1, \tilde{a}_2, \tilde{a}_{3\mathrm{I}}, \tilde{a}_{3\mathrm{Q}}, \tilde{a}_{4\mathrm{I}}, \tilde{a}_{4\mathrm{Q}}, \tilde{k}_1$, and $\tilde{k}_2$ refer to the estimates of the ideal coefficients without tilde ($\tilde{}$) used in Section II. The mitigation structure is only able to remove the distortion stemming from the strong blocker(s) in $\hat{x}(n)$. Therefore, it does not take into account the intermodulation between the blocker(s) in $\hat{x}(n)$ and some weaker signals in $d(n)$. However, this is not a relevant limitation in practice, because these IMD components are always relatively weak.

It is worth noticing that the bandstop filter of the main path filters out the strongest blocker(s), which is desirable in order to provide the best possible circumstances for the adaptive filters to converge. However, in some systems it might be desirable to have the strongest blocker(s) present after mitigating the distortions, e.g., if they are communication signals of interest. This is accomplished by adding back the blocker(s) after mitigation. In practice, this means adding the bandpass filter output $\hat{x}(n)$ to the output of the entire mitigation structure as is indicated by the dashed arrow line at the top of Fig. 3. This optional feature is employed in the examples of Section IV as is obvious from its spectrum figures.

With slight modifications, the mitigation structure in Fig. 3 can be used for enhancing weak *individual IF carrier demodulation*. In this scenario, the motivation is to remove distortions from a certain narrow band, which contains a weak signal of interest suffering from interference stemming from strong neighboring signals. Here, the narrowband signal refers to an information-bearing signal that does not occupy the entire reception bandwidth, but there are also neighboring signals digitized at the same time, e.g., for flexible digital channel selection filtering purposes. In practice, the cleaning of the certain band means that the bandstop filters in Fig. 3 should be changed to bandpass filters and correspondingly also the bandpass filter should be replaced with an appropriate bandstop filter. Thus, the signal band of interest is selected with the bandpass filter and the bandstop filter is then selecting the rest of the bandwidth for modeling the distortion. However, it is also possible to use a bandpass filter instead of the bandstop filter to pick up the strongest blockers and only use them for modeling the distortion to the band of interest. This would be preferable in a sense that those blockers are causing most of the interference. Also, the distortion regeneration would be more accurate since less distortion is passed to the modeling stage, which would cause additional distortion components not actually present in the received signal.

Designing the bandsplit filters needed in the mitigation structure is omitted from this paper as this is essentially a classical digital filter optimization task for given requirements. This depends on the specific use case, the receiver structure, and the desired complexity of the implementation. A general guideline is that the strongest blocker(s) should be extracted and used in the reference path for the distortion regeneration. This is because the strongest blockers cause also the strongest, and therefore, potentially the most harmful distortion. The selection of the strongest blocker(s) can be based, e.g., on a simple energy detector decisions. It is possible to select only a single blocker and design the filters with only one passband/stopband. However, it is equally feasible to select more than one blocker with a multiband filter. This is basically a matter of filter design and does not affect the processing in the reference path in any way, i.e., the nonlinearity modeling structure remains the same.

Although the structure in Fig. 3 explains conveniently the mitigation concept, it has one severe practical limitation. It works perfectly if the exact coefficients are known a priori. However, this is usually not the case in practice. Online adaptation of the coefficients is thus desired and even required in SDR applications. However, the coefficient adaptation cannot be done directly with this structure, because there are cascaded coefficients that should be adapted simultaneously. For example, if RF nonlinearity coefficients $\tilde{a}_1$ and $\tilde{a}_2$ are adapted alone, they converge to optimal values for completely removing the frequency components having RF nonlinearity contribution. However, as the analysis in Section II shows, the same frequency components have also BB nonlinearity contribution, which should not be removed. This is because it becomes difficult to adapt the BB nonlinearity coefficients $\tilde{a}_{3\mathrm{I}}, \tilde{a}_{3\mathrm{Q}}, \tilde{a}_{4\mathrm{I}}$, and $\tilde{a}_{4\mathrm{Q}}$, when some of the BB distortion components are not anymore in the signal to be cleaned. The same problem occurs if the BB distortion is removed before the RF distortion. The common frequency content in the RF and BB distortions implies time-domain correlation between the distortion components when they originate from the same original blocker(s). It is known that this type of correlation affects the adaptation process [28]. In addition, inefficiency

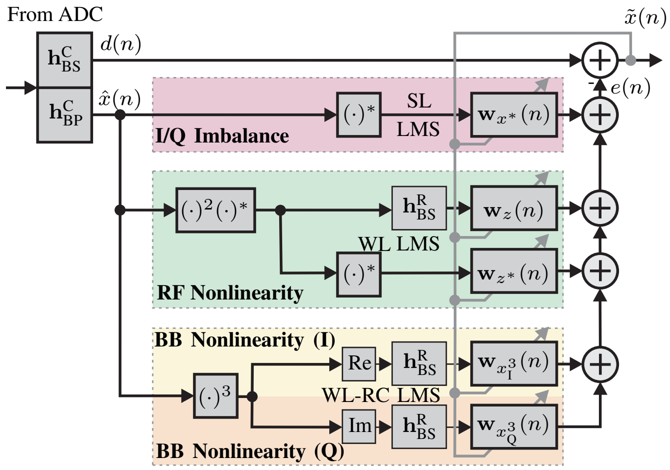

Fig. 4. Parallel adaptive digital mitigation structure for cascaded RF and BB nonlinearities with mixer and BB I/Q imbalance.

of removing only either RF or BB distortions is illustrated in Subsection IV-B with a two-tone simulation example. This motivates us to further develop the mitigation structure, as outlined in Subsection III-B below.

B. Practical Mitigation Structure

Since the online adaptation of cascaded nonlinearity coefficients is not feasible, the mitigation structure of Fig. 3 has to be modified so that all the coefficients can be adapted simultaneously. This becomes possible when the RF nonlinearity and mixer I/Q imbalance blocks are moved *in parallel* with the BB nonlinearity block in the reference generation processing. In principle, this means separate parallel branches for all the distortion terms derived in Subsection II-C. However, further optimization to reduce complexity can be performed since not all the terms are relevant in practice. The final proposed mitigation structure is illustrated in Fig. 4 and is explained in the following paragraphs in more detail. The complex bandpass, real bandstop, and complex bandstop filters are denoted by $\mathbf{h}_{\mathrm{BP}}^{\mathrm{C}}$, $\mathbf{h}_{\mathrm{BS}}^{\mathrm{R}}$, and $\mathbf{h}_{\mathrm{BS}}^{\mathrm{C}}$, respectively. In addition, please note that true multitap adaptive filters (AFs) are also now deployed, to support frequency-selective nature (memory) of associated nonlinearities.

Only the most important distortion terms and their complex conjugates should be selected from Table I for the mitigation structure. There are two reasons for that: 1) less terms means smaller computational burden, and 2) very weak terms are buried below the receiver noise level, which makes them negligible and impedes the convergence of AFs. Therefore, this paper proposes to use the terms in Table II for the mitigation, which should be enough for any practical DCR. The terms follow from the derivations in Section II, but hats ($\hat{}$) are used to indicate that these are calculated from $\hat{x}(n)$, which is the output of the filter $\mathbf{h}_{\mathrm{BP}}^{\mathrm{C}}$ containing the blocker(s). In fact, $\hat{x}(n)$ is only an estimate of the distortion-producing blocker(s), which also suffer(s) from in-band distortion.

We first discuss the role of the different essential terms on intuitive level, and describe the exact learning methods then later in Subsection III-C. Term 1 is usually the strongest

TABLE II
SELECTED TERMS FOR PARALLEL MITIGATION STRUCTURE

Term #	Equation	Filtering	Vector Notation
Term 1	$\hat{x}^*(n)$	SL	$\mathbf{s}_{x^*}(n)$
Term 2	$\hat{z}(n)$	WL	$\mathbf{s}_z(n), \mathbf{s}_{z^*}(n)$
Term 3	$\hat{x}^3(n)$	WL-RC	$\mathbf{s}_{x_{\mathrm{I}}^3}(n), \mathbf{s}_{x_{\mathrm{Q}}^3}(n)$

and its power level is easy to estimate from the power level of $\hat{x}(n)$ and image rejection ratio (IRR) of the receiver. Third column of Table II indicates whether the terms should have strictly-linear (SL), widely-linear (WL), or reduced-complexity widely-linear (WL-RC) filtering. In general, the term "widely-linear" refers to processing where both direct and conjugated signals are processed and finally summed together [26], [29]. Regarding Term 1, SL filtering means that the mitigation structure finds complex AF coefficients for $\hat{x}^*(n)$. Term 2 is important since it has contributions from both RF and BB nonlinearities. If any I/Q imbalance occurs, the complex conjugate of Term 2 is also significant. Therefore, WL filtering is applied for Term 2 meaning that separate complex AFs for $\hat{z}(n)$ and $\hat{z}^*(n)$ are deployed. After generating $\hat{z}(n)$, it has to be filtered with $\mathbf{h}_{\mathrm{BS}}^{\mathrm{R}}$ in order to remove spectral content from the original blocker frequency band. This is necessary since otherwise the adaptive algorithm would be misadjusted as $d(n)$ does not have any content in the original blocker frequency band. Regarding $\hat{z}^*(n)$, it is not necessary to use $\mathbf{h}_{\mathrm{BS}}^{\mathrm{R}}$, because it does not contain energy in the original blocker frequency band anyway. The WL filtering is also used for Term 3, which stems from the BB nonlinearity. Both $\hat{x}^3(n)$ and $[\hat{x}^*(n)]^3$ should be filtered with $\mathbf{h}_{\mathrm{BS}}^{\mathrm{R}}$. Therefore, it is actually possible to reduce the complexity of finding AFs for these terms by exploiting the WL-RC approach, which is discussed later in this subsection.

The selected terms in Table II are justified, because they cover the strongest distortion terms. In addition, the terms do not have much spectral overlapping. This is important since all the nonlinear distortion originates from the same blocker(s) and thus has also time-domain correlation, as mentioned earlier. By minimizing the spectral overlapping of the distortion terms, the time-domain correlation between the distortion terms is minimized. This feature is important for the convergence of adaptive algorithms used for finding the AFs.

Terms 4–9 from Table I are not used in the mitigation structure of Fig. 4 because they are negligible when receiver nonlinearities have physically realistic values. The minimal contribution of those terms is easy to understand, because they are 5th, 7th, and 9th order terms, whereas others have a maximum order of three. However, the order of importance for the meaningful terms can slightly vary. This claim is based on our own experiments as discussed in Section IV. In the end, the receiver noise level usually dictates which terms are negligible and which are not. Overall, the mitigation structure in Fig. 4 is a carefully found compromise between the implementation complexity and the achievable mitigation performance, and is directly stemming from the nonlinear distortion analysis provided in Section II. More discussion and examples about the mitigation is provided in Section IV.

It is also important to understand that the sample rate used during the mitigation processing limits the nonlinearity modeling possibilities. If the ADC has the sampling rate f_s and the same rate is used also in the mitigation structure, the original blocker frequencies must be less than $f_\mathrm{s}/6$ in order to model the third-order nonlinearities correctly, i.e., without aliasing. This limitation comes from the fact that third-order nonlinear distortion occupies three times the original signal bandwidth. Naturally, aliasing does not occur in the analog BB of the receiver and, therefore, it has to be avoided also in the distortion modeling in digital domain. The limitation can be avoided by temporarily increasing the sample rate in digital processing while applying the nonlinearities in the mitigation branches of Fig. 4.

C. Practical Least-Mean-Square Based Learning Rules

The impulse response length, say M, of the AFs for all the distortion terms in Fig. 4 depends on the memory effects of the receiver front-end. The analysis in Section II considers memoryless situation ($M = 1$) to keep it concise. However, using $M > 1$ in the proposed mitigation structure is straightforward in practice and typically required as discussed in Subsection IV-E. According to our experiments, small M should be enough in many applications. However, if large M is required for proper modeling, sparse delay tap filters may provide better accuracy with lower complexity than the traditional non-sparse AFs described in this subsection [30].

As the goal of the mitigation is in general to minimize the spurious energy, the adaptation of the AFs can be performed, e.g., by using the least-mean square (LMS) algorithm or any similar adaptive algorithm [28]. The WL version of the LMS algorithm is extensively exploited in the current literature as discussed in [29] and references therein. Finding two complex AFs for a signal using the WL LMS would imply an increased computational complexity compared to the SL version of the LMS. However, it is possible to reduce the complexity of the WL LMS to that of the SL LMS. It is proven in [31] that the WL-RC LMS is able to provide the same mean-square error and convergence rate while reducing the computational complexity to the level of the SL LMS. Due to these pleasant features, the reduced-complexity WL LMS is also exploited in this paper as is indicated in Fig. 4. The intuition behind the reduced complexity is the fact that instead of finding two complex AFs for a complex signal it is equivalent to finding complex AFs for the real and imaginary parts of the signal [26], [31]. That is to say, finding filters $\mathbf{w}_{x^3}(n)$ and $\mathbf{w}_{x_\mathrm{c}^3}(n)$ for

$$\mathbf{w}_{x^3}(n) * \hat{x}^3(n) + \mathbf{w}_{x_\mathrm{c}^3}(n) * [\hat{x}^*(n)]^3 \tag{18}$$

is equivalent to finding filters $\mathbf{w}_{x_\mathrm{I}^3}(n)$ and $\mathbf{w}_{x_\mathrm{Q}^3}(n)$ for real and imaginary parts of $\hat{x}^3(n)$, i.e.,

$$\mathbf{w}_{x_\mathrm{I}^3}(n) * \mathrm{Re}[\hat{x}^3(n)] + \mathbf{w}_{x_\mathrm{Q}^3}(n) * \mathrm{Im}[\hat{x}^3(n)]. \tag{19}$$

This is valid because the relationships between the filters are

$$\begin{aligned}\mathbf{w}_{x_\mathrm{I}^3}(n) =& \mathrm{Re}[\mathbf{w}_{x^3}(n)] + \mathrm{Re}[\mathbf{w}_{x_\mathrm{c}^3}(n)]\\ &+ j\{\mathrm{Im}[\mathbf{w}_{x^3}(n)] + \mathrm{Im}[\mathbf{w}_{x_\mathrm{c}^3}(n)]\}\end{aligned} \tag{20a}$$

$$\begin{aligned}\mathbf{w}_{x_\mathrm{Q}^3}(n) =& \mathrm{Im}[\mathbf{w}_{x_\mathrm{c}^3}(n)] - \mathrm{Im}[\mathbf{w}_{x^3}(n)]\\ &+ j\{\mathrm{Re}[\mathbf{w}_{x^3}(n)] - \mathrm{Re}[\mathbf{w}_{x_\mathrm{c}^3}(n)]\}\end{aligned} \tag{20b}$$

The computational complexity is smaller in (19), because two complex filters are applied for real-valued signals instead of complex-valued signals as is the case in (18).

Due to the WL filtering of Terms 2 and 3, there are in total five distortion branches in the mitigation architecture of Fig. 4. For joint coefficient learning purposes, the distortion branch signals are combined into one vector $\mathbf{s}(n)$, namely

$$\mathbf{s}(n) = \left[\mathbf{s}_{x^*}(n), \mathbf{s}_z(n), \mathbf{s}_{z^*}(n), \mathbf{s}_{x_\mathrm{I}^3}(n), \mathbf{s}_{x_\mathrm{Q}^3}(n)\right]^\mathrm{T}, \tag{21}$$

where the subscripts indicate the distortion branches. Term 1 vector is $\mathbf{s}_{x^*}(n) = [\hat{x}^*(n), \hat{x}^*(n-1), \ldots, \hat{x}^*(n-M+1)]^\mathrm{T}$, where M is the AF length. The vectors $\mathbf{s}_z(n)$, $\mathbf{s}_{x_\mathrm{I}^3}(n)$, and $\mathbf{s}_{x_\mathrm{Q}^3}(n)$ also include filtering with $\mathbf{h}_\mathrm{BS}^\mathrm{R}$ and hence $\mathbf{s}_z(n) = [\hat{z}_\mathrm{filt}(n), \hat{z}_\mathrm{filt}(n-1), \ldots, \hat{z}_\mathrm{filt}(n-M+1)]^\mathrm{T}$, where $\hat{z}_\mathrm{filt}(n)$ refers to the filtered version of $\hat{z}(n)$. Similar notation applies to $\mathbf{s}_{x_\mathrm{I}^3}(n)$ and $\mathbf{s}_{x_\mathrm{Q}^3}(n)$. Also the AFs are combined into one vector, namely

$$\mathbf{w}(n) = \left[\mathbf{w}_{x^*}(n), \mathbf{w}_z(n), \mathbf{w}_{z^*}(n), \mathbf{w}_{x_\mathrm{I}^3}(n), \mathbf{w}_{x_\mathrm{Q}^3}(n)\right]^\mathrm{T}, \tag{22}$$

where the subscript indicates the corresponding distortion branch and each individual AF has length of M. Notice that it is also very straightforward to deploy different AF lengths for different distortion terms, if e.g. RF and BB amplifier(s) contain different levels of frequency-selectivity.

The complete joint LMS algorithm for all the coefficients of the mitigation structure in Fig. 4 can be then formulated as follows. First, the AF vector $\mathbf{w}$ is initialized as

$$\mathbf{w}(0) = \mathbf{0}_{5M\times 1}, \tag{23}$$

if no a priori information is available, e.g., through device measurements. For all $n = 0, 1, 2, \ldots$ the combined AF output is

$$e(n) = \mathbf{w}^\mathrm{H}(n)\mathbf{s}(n). \tag{24}$$

Then the error calculation step is

$$\tilde{x}(n) = d(n) - e(n) \tag{25}$$

and finally the AF update is given by

$$\mathbf{w}(n+1) = \mathbf{w}(n) + \mathrm{diag}(\boldsymbol{\mu})\tilde{x}^*(n)\mathbf{s}(n), \tag{26}$$

where $\mathrm{diag}(\cdot)$ denotes a function for converting a vector to a diagonal matrix. The step-size vector $\boldsymbol{\mu}$ contains a different step size for every distortion branch, i.e., $\boldsymbol{\mu} = [\mu_{x^*}, \mu_z, \mu_{z^*}, \mu_{x_\mathrm{I}^3}, \mu_{x_\mathrm{Q}^3}]$, where the subscripts indicate the corresponding distortion branches.

Normalized least-mean square (NLMS) can in practice provide more robust convergence behavior and eases the tuning of the step sizes [28]. Therefore, this approach is used in the mitigation examples of Section IV. The only difference between LMS and NLMS is that the step sizes are scaled with the squared Euclidean norm of the corresponding signal vector and with a selectable coefficient. Consequently, the step-size vector for NLMS is

$$\boldsymbol{\mu}_{\mathrm{N}} = \left[\frac{\mu_{x^*}}{\alpha_{x^*} + \left\| \mathbf{s}_{x^*}(n) \right\|^2}, \ldots, \frac{\mu_{x_{\mathrm{Q}}^3}}{\alpha_{x_{\mathrm{Q}}^3} + \left\| \mathbf{s}_{x_{\mathrm{Q}}^3}(n) \right\|^2} \right], \quad (27)$$

where the additional selectable constants are $\boldsymbol{\alpha} = [\alpha_{x^*}, \alpha_z, \alpha_{z^*}, \alpha_{x_{\mathrm{I}}^3}, \alpha_{x_{\mathrm{Q}}^3}]$. These constants are included due to numerical difficulties in case the power of the distortion estimates is very low and the denominator in (27) is close to zero.

D. Computational Complexity

The computational complexity for creating the distortion estimates consists of 16 real multiplications and 8 real summations used in the complex-valued power operations shown in Fig. 4. In parallel, the cost of the adaptation is defined by the AF length M. For a single iteration of complex LMS the required operations are $8M + 2$ real multiplications and $8M$ real summations in the SL and WL-RC cases [31]. With complexity of a conventional LMS AF being $2M+1$ complex multiplications and $2M$ complex summations per iteration [28], the WL LMS takes $16M + 2$ real multiplications and $16M$ real summations [31]. When combined according to Table II, the overall complexity with the LMS adaptation is $32M + 6$ real multiplications and $32M$ real summations. Employing complex NLMS algorithm introduces an additional burden of $2M$ real multiplications and M real summations for calculating the squared euclidean norm and 1 real division and 1 real summation for finally scaling the step-size, per distortion estimate. Thus, the final number of operations for the adaptations is $42M$ real multiplications, 5 real divisions and 21 real summations.

On top of this, there is the computational cost of the five filters applied in the mitigation structure. There are two complex-valued filters operating on complex-valued signals (namely, $\mathbf{h}_{\mathrm{BP}}^{\mathrm{C}}$ and $\mathbf{h}_{\mathrm{BS}}^{\mathrm{C}}$) and one real-valued filter ($\mathbf{h}_{\mathrm{BS}}^{\mathrm{R}}$) operating once on a complex-valued signal and twice on a real valued signal, as shown in Fig. 4. Assuming all the filters are of order P and direct-form finite impulse response (FIR) structure (P multiplications and $P - 1$ summations for real filter and real signal), this introduces $12P$ real multiplications and $4P + 8(P - 1) = 12P - 8$ real summations assuming direct convolution. This cost can, however, be reduced, e.g., by precomputing the fast Fourier transforms (FFTs) of the filters and doing the filtering in frequency domain, if efficient FFT implementation is available. The details of filtering optimization are not considered herein and can be further checked, e.g., from [32].

Finally, the number of real multiplications, summations and divisions is summarized in Table III. In addition, the delay of the proposed algorithm, being $P+M$, is in practice dictated by the filter order P because it is usually significantly higher than the AF order M. A practical field-programmable gate array (FPGA) implementation of purely digital mitigation algorithm but considering only the RF LNA nonlinearity and hence being a greatly simplified setup, can be found in [15].

TABLE III
THE NUMBER OF REAL MULTIPLIERS, REAL ADDERS AND REAL DIVIDERS USED IN THE MITIGATION STRUCTURE

Operation	# Ops.	Muls	Adds	Divs
Ref. Modeling		16	8	-
SL LMS	1	$8M + 2$	$8M$	-
WL LMS	1	$16M + 2$	$16M$	-
WL-RC LMS	1	$8M + 2$	$8M$	-
NLMS Scaling	5	$10M + 5$	$5M + 5$	5
Static Filtering	5	$12P$	$12P - 8$	-
Overall		$12P + 42M + 27$	$12P + 37M + 5$	5

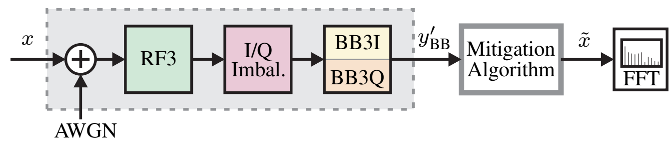

Fig. 5. Simulation architecture for performance evaluation of the mitigation algorithm in MATLAB.

IV. PERFORMANCE SIMULATIONS AND MEASUREMENTS

This section provides simulation and measurement results which evaluate the performance of the proposed mitigation architecture for the cascaded third-order nonlinearities with I/Q imbalance. We also provide explicit comparisons to RF-only and BB-only mitigation approaches, reported earlier in literature, to illustrate and quantify the achievable gain from the proposed joint processing.

A. Simulation Setup

First, simulations of a complete receive chain are performed in MATLAB. The basic architecture is illustrated in Fig. 5. Signal generation and processing take place at BB equivalent level. First, the input signal passes the additive white Gaussian noise (AWGN) source, the RF nonlinearity, the I/Q imbalance block, and the BB nonlinearity. All these components are applied to mimic the DCR front-end. In the blocker signal simulations, the signal-to-noise ratio (SNR) is 61 dB for the entire BB bandwidth of 25 MHz. The IRR is set to 30 dB, a value being realistic for an integrated DCR front-end [1]. The total composite signal, including noise and distortions, is then further processed by the mitigation algorithm presented in Subsection III-B.

Two-tone signals and binary phase shift keying (BPSK) modulated signals have been generated as input signals, in order to verify the algorithm with continuous wave and modulated signals. Throughout the paper, simplified signal configurations have been applied that do not consider detection of a specific information signal. Instead, results are interpreted from wideband nonlinear distortion mitigation use case perspective. Hence, the complete BB spectrum needs to be cleaned from distortions and only the strong input signal(s) should be left after mitigation. This is achieved by adding the original blocker(s) back to the output of the mitigation structure, as discussed in Section III.

Single-tap complex AFs are used in the simulations, as also the deployed circuit components models are memoryless. After mitigation, block-wise FFT with 1024 points is applied to analyze and illustrate the remaining nonlinear distortion. In the following subsections, the last one of 29 FFT blocks is shown in which the convergence of the coefficients is guaranteed.

As a figure of merit, the *mitigation gain* for the BPSK case is computed as the reduction in average signal power outside the original input (blocker) frequency band. Also the mirror-image band is excluded from the mitigation gain calculations as the focus is on the reduction in nonlinear distortion power. For the two-tone case, *average suppression of nonlinear distortion components* is used as a figure of merit, meaning that average power decrease only on the specific frequencies containing the nonlinear distortion is considered. For measurements, this means the average power decrease on the third-order distortion components whereas in the simulations also the mirrors of these components are taken into account as they also appear above the noise floor (see Fig. 7).

B. Two-tone Blocker Input

In order to demonstrate the most relevant distortion estimates, the power levels of Terms 1–6 (as listed in Table I) are next studied by means of a two-tone simulation. To keep the illustration simple, mirror images are not included in this particular example. In order to visualize all terms with respect to their power level, noise has been excluded in this particular simulation. Fig. 6a depicts the distortion estimates for dominating RF nonlinearity, i.e., having $|a_2| > |a_4|$. Vector $\mathbf{a}$ in the caption of Fig. 6 is defined as $\mathbf{a} = [a_1, a_2, a_3, a_4]$, where $a_3 = a_{3\mathrm{I}} = a_{3\mathrm{Q}}$ and similarly for a_4. The applied parameters correspond to the ones defined in Table IV. In Fig. 6, Term 2 is stemming from both the RF and BB distortion whereas the other terms are due to the BB nonlinearity only, as discussed in Sections II and III. Variable $\hat{x}$ (Term 1) depicts the BB spectrum of the filtered blocker signal that serves as an input for the reference nonlinearity. It is apparent that the Terms 2 and 3 are the most significant ones in this case. It is sufficient to consider common spectral content of multiple terms by only one term, as the AF adapts the term to the total distortion at these frequencies. Thus, only those distortions of higher-order terms need to be considered that have not been covered by lower-order terms. However, in this case, frequency components added by Terms 4–6 are 80 dB or more below the input power level and, therefore, likely to be masked by noise in practice. In addition, SNR of a typical ADC is approx. 60–80 dB depending on its resolution, hence making all terms below -80 dBFS to disappear below quantization noise. Fig. 6b illustrates then the power levels for dominating BB nonlinearity case, i.e., $|a_2| < |a_4|$. The same parameters values from Table I are used, but the gain and input-referred third-order intercept point (IIP3) of the RF stage are applied now for the BB and vice versa in order to make the BB dominating. In Fig. 6b, Term 2 and Term 3 are almost equally strong, but still these two terms are the most significant. The observations support the analysis in Sections II and III, and are assumed to be valid for practical values of RF and BB nonlinearities.

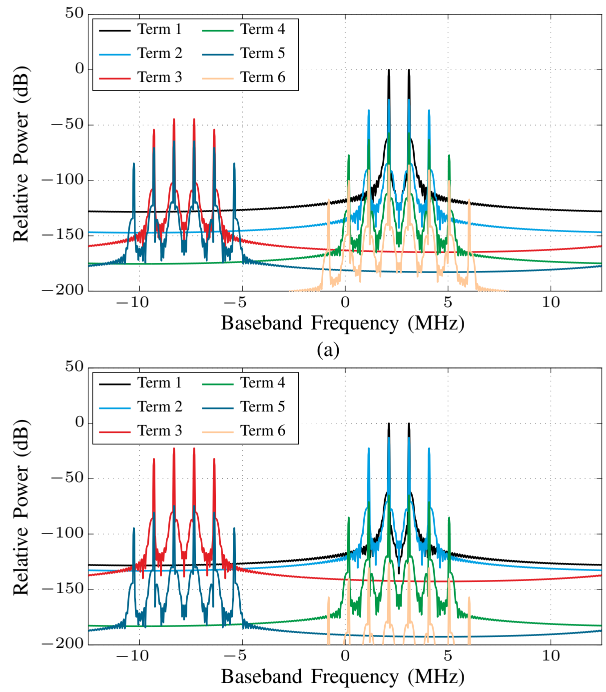

Fig. 6. Power levels of distortion estimates with (a) dominating RF nonlinearity $\mathbf{a} = [5.62, -(84351 + j74391), 3.16, -1588.7]$ and (b) dominating BB nonlinearity $\mathbf{a} = [3.16, -1588.7, 5.62, -(84351 + j74391)]$. For simplification, mirror terms are not visualized.

TABLE IV
PARAMETERS OF THE TWO-TONE SIMULATION

$IIP3_{\mathrm{RF}}$	-10 dBm	
G_{RF}	15 dB	
$IIP3_{\mathrm{BB}}$	$+6$ dBm	
G_{BB}	10 dB	
P_{input}	-30 dBm	
$\mathbf{a}$	$[5.62, -(84351 + j74391), 3.16, -1588.7]$	
g_{m}	0.99	IRR $\approx$ 30 dB
ϕ_{m}	$0.0628 \,\widehat{=}\, 3.6°$	
$\boldsymbol{\mu}$	$[1, 1, 0.01, 1, 1]$	
$\boldsymbol{\alpha}$	$[10^{-9}, 10^{-8}, 10^{-4}, 10^{-9}, 10^{-8}]$	

The parameters for the actual performance simulations, including also mirror effects, are summarized in Table IV, where the coefficients of the nonlinearity models and the I/Q imbalance coefficients are taken into account according to (7), (13a), (13b), and (9). It is noteworthy that phase distortions created by LNA and mixer are considered by complex coefficients a_2, k_1, and k_2. The coefficients $a_1 \ldots a_4$ have been computed based on practical values for gain and IIP3 of the RF and BB amplifiers [12].

Fig. 7a illustrates the BB spectrum with a two-tone input before and after proposed mitigation. With the two-tone input, 16 signal components are created in total due to the receiver nonlinearities and I/Q imbalance. The mirror images appear 30 dB below the original tones, whereas the strongest distortion components due to the nonlineaties are 36 dB below the original tones. First, the two-tone signal

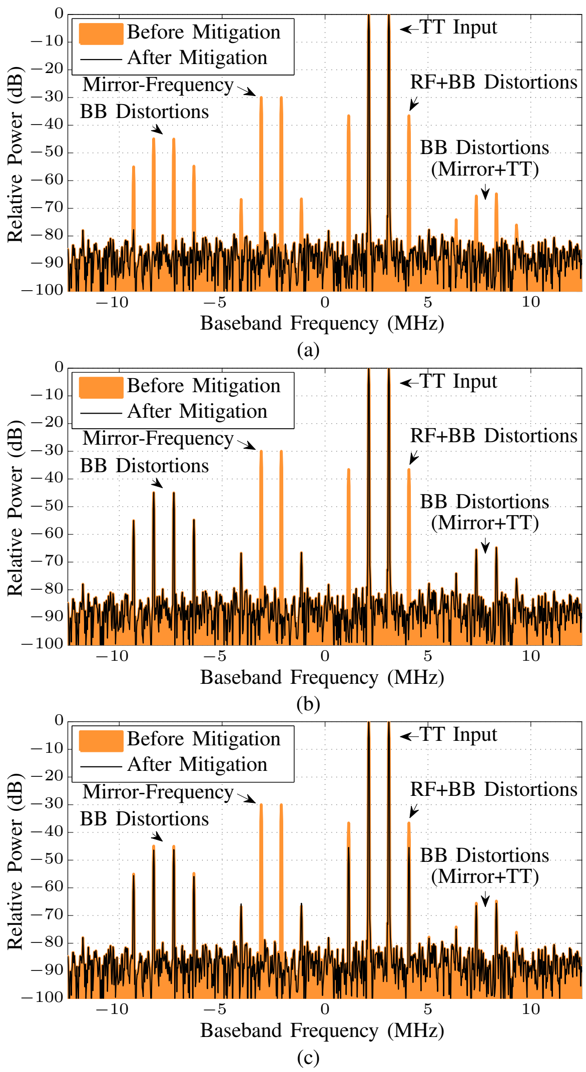

Fig. 7. Simulation results with two-tone input and mitigation with (a) the proposed cascaded model, (b) RF-only model, and (c) BB-only model.

is distorted by the RF amplifier, causing IMDs nearby the original baseband-equivalent frequency at 2.6 MHz (center of the two tones). Second, mirror components of the original tones and the RF distortion components appear due to down-converting mixer I/Q mismatches. Third, the original tones plus the RF distortions and their respective mirror components are all further distorted by the BB I and Q nonlinearities. This creates distortions at the third harmonic zone of the original signal on the left side of the spectrum around -7.8 MHz and adds distortion around the original tones. In addition, the BB nonlinearity causes harmonics and IMD originating from the mirror components which then appear as low-power tones around $+7.8$ MHz. Furthermore, the BB distortions can have respective mirror components, if there is I/Q imbalance in the BB branches, although these components are very likely to remain below the noise floor in practice. In fact, the mirror components of the main RF and BB distortions are mitigated with the WL filters in the proposed structure if they do appear. Furthermore, AM/PM distortion caused at the RF amplifier [24] and phase mismatch introduced by the mixer are taken into account by the complex implementation of the AFs.

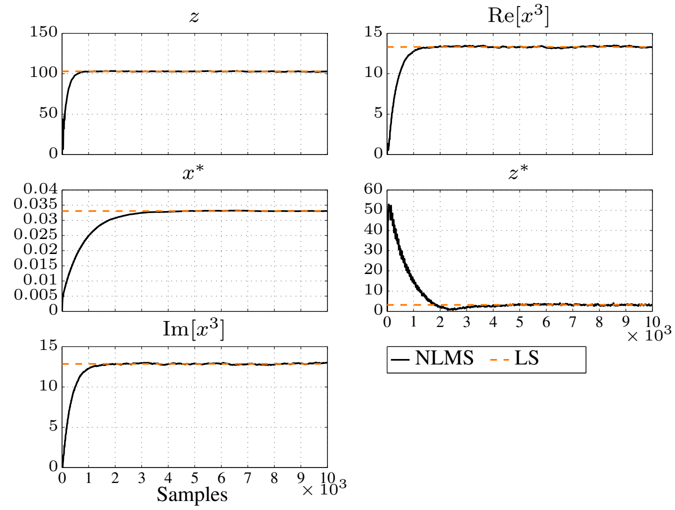

Fig. 8. Adaptation of the filter coefficients with two-tone input (magnitude of complex coefficients).

In this example setting, the average suppression of nonlinear distortion components with the proposed joint processing is 32.6 dB for Fig. 7a, fully canceling all distortion and mirror components. Fig. 8 illustrates the adaptation of the AFs using NLMS algorithm, as discussed in Subsection III-B. NLMS has been selected instead of conventional LMS as it usually provides more robust convergence behavior [28]. In addition, the selection of the step size is more simple due to the normalization to the power of the distortion estimates, which may vary by several orders of magnitude. The deployed NLMS parameters are given in Table IV. In Fig. 8, the magnitudes of the adapted complex coefficients are shown together with the corresponding least squares (LS) solutions for the coefficients which are indicated with dashed lines. Basically, there is a good match between the steady-state solution of the adapted coefficients and the LS solutions. The coefficients are converged after approx. 3000 samples.

In order to further demonstrate the significance of the cascaded nonlinearity model for mitigation performance, simulations with only the RF or only the BB model for mitigation are shown for the two-tone input. In the observation generation, however, the same full cascaded model is used as earlier, mimicking a realistic analog DCR front-end. In Fig. 7b, only the mirror image of the original signal and RF distortions have been treated (Terms $\hat{x}^*$ and $\hat{z}$). Further distortions at the BB have not been taken into account here, i.e., there are no distortions estimates for mitigating the components, e.g., in the third harmonic zone. In Fig. 7c, on the other hand, only the mirror image of the original signal and the third-order nonlinearity at the BB are considered (Terms $\hat{x}^*$, $\mathrm{Re}[\hat{x}]^3$, and $\mathrm{Im}[\hat{x}]^3$). The poor performance of the BB-only model is due to the fact that it is unable to take into account the RF distortion, which partially appears at the same frequencies as BB distortion. In addition, the BB-only model is unable to take into account harmonics and IMD of the mirror image. Only if the RF and mixer distortion is mild, the BB-only model is

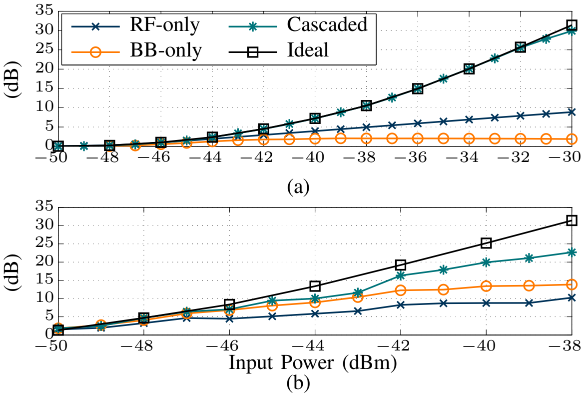

Fig. 9. Average suppression of nonlinear distortion components for different mitigation models, obtained with (a) simulated and (b) measured data.

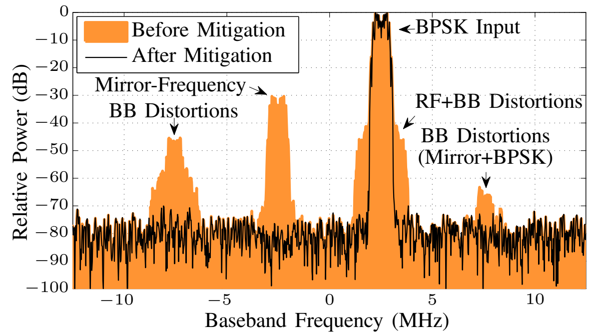

Fig. 10. Simulation results with BPSK input and mitigation with the proposed cascaded model.

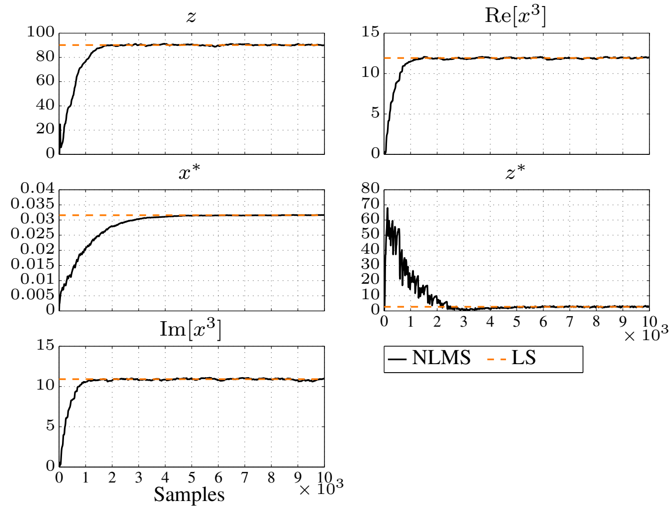

Fig. 11. Adaptation of the filter coefficients with BPSK input (magnitude of complex coefficients).

able to perfectly remove all the occurring BB distortion [9]. Therefore, the cascaded nonlinearity model proposed in this paper clearly outperforms the RF-only and BB-only models considered in the current literature.

The average suppression of nonlinear distortion components vs. the power of the two-tone input achieved with the different models, and the ideal suppression, indicating how much spurious power has been added due to receiver nonlinearity, are illustrated in Fig. 9a. With the deployed analog components, there is almost no IMD generated up to input power -46 dBm and the mirror-frequency interference x^* is dominating. All the models include mitigation of the mirror with Term 1, hence, equal mirror suppression is achieved at these low power levels. Therefore, the mirror band is excluded from the mitigation gain calculations in order to better show the suppression of nonlinear distortion. With rising input power, the generated RF and BB distortions raise in Fig. 9a, and some suppression is achieved with the RF-only and BB-only models. However, the BB-only model is performing poorly due to the strong RF nonlinearity, which only partially accommodates the same frequencies. The cascaded model follows the ideal suppression, indicating that all nonlinear distortion products plus mirror terms are essentially canceled. To sum up, the total cascaded model provides much better performance than the RF-only or BB-only nonlinearity model because of their fundamental shortcomings. Using the BB-only model, i.e., the third-order term of the I and Q reference signal, is exactly the procedure followed in the state-of-the-art literature [7], [9], while RF LNA oriented results are reported in [12]. These results show that proper modeling of the underlying receiver architecture is essential to achieve improved mitigation performance in a broad variety of applications.

C. BPSK Blocker Input

The results with the BPSK input are shown in Fig. 10. The BPSK signal is generated with a raised-cosine pulse-shaping filter, with a roll-off factor of 0.5 and a symbol rate of approx. 788 ksym/s. These numbers have been chosen arbitrarily to generate a simple modulated blocker signal with approx. 1 MHz bandwidth. The parameters for the BPSK simulation are otherwise exactly the same as for the two-tone case summarized in Table IV. The root-mean-square power has been chosen to be equal to that in the two-tone case, whereas the peak-to-average power ratio (PAPR) of the BPSK signal is higher than that of the two-tone ($PAPR_{\mathrm{BPSK}} = 4.1$ dB vs. $PAPR_{\mathrm{TT}} = 3.01$ dB). It should be noted that the peak values are important in determining the level of distortion. Fig. 11 illustrates the adaptation of the coefficients using NLMS. The steady-state value is again reached at approx. 4000 samples, resulting in a mitigation gain of 20.4 dB. The results with BPSK input verify that the proposed algorithm is able to mitigate distortions induced by modulated blocker waveforms.

D. High-PAPR Input Signals

Especially in CR applications, typically high PAPR is encountered. Besides the fact that modern communications waveforms tend to have high PAPR, also receiving multiple low-PAPR signals with one receiver chain will cause the overall waveform to have high PAPR. As discussed in Subsection III-A, the proposed nonlinearity mitigation algorithm is able to handle situations with multiple blocker signal carriers while the computational complexity stays almost the same. This is due to the fact that only the band-splitting stage filters have to be designed to have multiple passbands while the

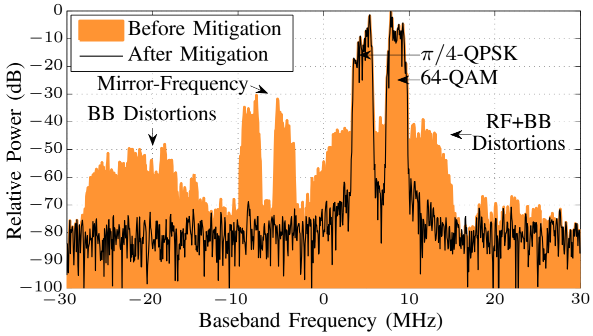

Fig. 12. Simulation with two single-carrier signals ($\pi/4$-QPSK and 64-QAM) at -30.67 dBm, PAPR = 7.54 dB, and mitigation with proposed cascaded model.

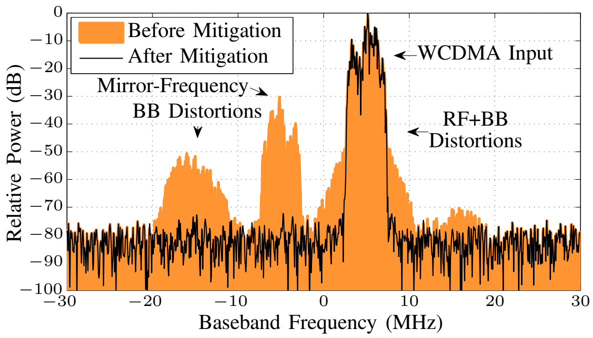

Fig. 13. Simulation with a WCDMA input at -31.89 dBm, PAPR = 10.95 dB, and mitigation with proposed cascaded model.

nonlinearity modeling and adaptation stay the same.

In order to verify the feasibility of the approach under high-PAPR conditions, two more simulation examples (two single-carrier signals, one WCDMA signal) are illustrated in Fig. 12 and Fig. 13 providing a mitigation gain of 20.9 dB and 16.6 dB, respectively. In order to make the simulation scenarios even more realistic, a frequency-selective Extended ITU Vehicular A channel is used [33]. Essentially the channel does not affect the mitigation performance, but may slightly increase fluctuations in AF coefficient adaptation behavior. The channel effects are discussed more in Section V.

The nonlinearity mitigation algorithm is able to handle high-PAPR waveforms since the nonlinearity modeling itself is not depending on PAPR. Therefore, it is justified to say that the proposed algorithm is suitable and effective in CR applications. However, it is worth noticing that challenges due to the amplifier saturation or ADC clipping may occur in practice. If the signal is pushed to the highly nonlinear region of the receiver, the nonlinearity modeling should be changed drastically and hence the proposed algorithm as it is may not provide the optimal mitigation performance. The changes to the nonlinearity modeling could include, e.g., higher than third-order polynomials. Nevertheless, this problem is fundamentally challenging as part of the signal information is lost in saturation/clipping process.

E. Experimental Evaluation with RF Measurements

Real-world measurements are also conducted to demonstrate and verify the mitigation capabilities of the proposed solution

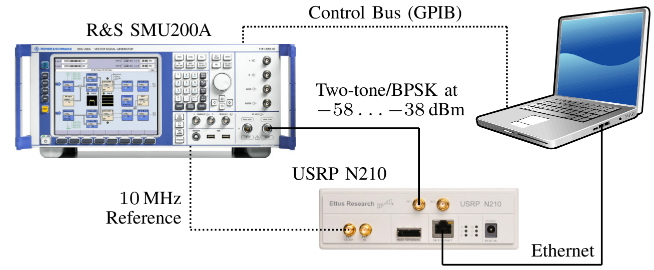

Fig. 14. Sketch of the two-tone and BPSK measurement setup.

with true RF signals and components. The automated setup for the experiments with the aforementioned signal scenarios is illustrated in Fig. 14. A vector signal generator of type Rohde & Schwarz SMU200A is used to generate the two-tone and BPSK signals. Before running measurements with an SDR under test, the spectral purity of the generator was checked with a conventional spectrum analyzer, as signal generators also exhibit a limited linearity. The generator itself has an SFDR better than 70 dB, i.e. a very clean signal can be provided to the device under test. The SDR USRP N210 with the wideband WBX front-end [18] is used as a receiver. Signal generator and receiver are synchronized using a 10 MHz reference signal, enabling coherent sampling for precise power measurements.

The WBX is a typical DCR front-end with a low-IF architecture, providing a tuning range from 70 MHz to 2.2 GHz. That is, from the perspective of a single signal of interest, the waveform is I/Q down-converted to a low-IF first, and subsequently down-converted to zero-IF in the digital domain. This is performed by a numerically controlled oscillator on an FPGA if the desired center frequency is not directly within the frequency grid of the analog local oscillator. The analog BB bandwidth of the daughterboard is 40 MHz, however, the transferable bandwidth to the host computer is limited to 25 MHz due to the gigabit Ethernet interface. The nonlinear behavior of the WBX front-end is already known from prior studies [7]. The IIP3 of the total receiver including RF, BB and ADC nonlinearity is 13.8 dBm on average, indicating a very good linearity in general. Moreover, the power of nonlinear distortions is independent from the chosen center frequency. The WBX has been chosen among a variety of USRP daughterboards as it provides a low noise figure (NF) of 5 dB, allowing observation of different distortion components.

Fig. 15a illustrates the mitigation performance achieved with a two-tone input. The tone frequencies are the same as in simulations and have been chosen within the grid of the 1024-point FFT. The generator power and the PAPR of the signal are -39 dBm and 3.06 dB, respectively. The center frequency of the receiver is 200 MHz, the BB bandwidth being 25 MHz. By using two taps for the AFs, the average suppression of nonlinear distortion components is 25.4 dB in Fig. 15a. The additional taps have been introduced, because the real receiver suffers from memory effects that are excluded in the simulations. The obtained suppression of nonlinear distortion components at different input power levels for the two-tone case are illustrated in Fig. 9b. Compared to simulations, RF

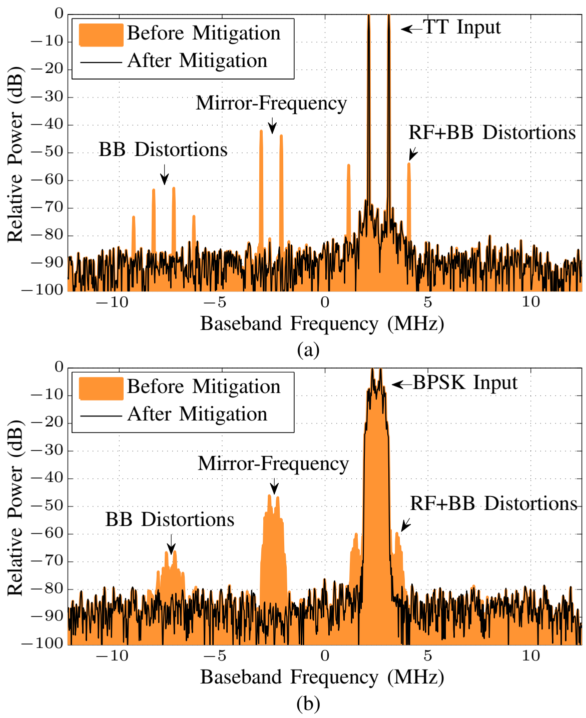

Fig. 15. Mitigation performance achieved with measured data in case of (a) two-tone input (at -39 dBm) and (b) BPSK input (at -44 dBm).

distortion is milder in measurements, explaining the relatively high suppression obtained by the BB-only model. However, the cascaded model still provides the best performance.

Similar mitigation performance is achieved with the BPSK signal shown in Fig. 15b. Here, the center frequency and the BB bandwidth are 570 MHz and 25 MHz, respectively. The BPSK signal has been generated with the same parameters as used in simulations, and the generator power and PAPR are -44 dBm and 3.35 dB, respectively. A mitigation gain of 7.1 dB is achieved using two taps for each AF.

To sum up, the co-existence of RF and BB distortions has been verified through real-world measurements, demonstrating the effectiveness of the proposed cascaded model. The suppression of the different distortion components is significantly better with the joint mitigation of the RF and BB stage nonlinearities, compared to the previous solutions presented in the literature which employ a model for only either of the stages. Moreover, joint mitigation of nonlinear distortions and corresponding mirror components due to I/Q imbalance has been demonstrated by measurements. Thus, the proposed mitigation method provides a high-performance linearization solution for complete wideband DCR chains, enabling flexible sensing and processing of the RF spectrum in radio communication and radar devices.

V. Results and Discussion

The results presented in Section IV show a very good match between the cascaded model in simulations and the real behavior in measurements. This confirms that the cascaded model addresses the most relevant distortions created by the DCR architecture. Thus, a complete model has been found capturing all essential distortions in the receiver chain. In general, only distortions that are created by the reference model can be mitigated with the AFs. In prior works, either distortions at RF or BB have been considered, but not together in a joint model. Adding more taps to the AF would not compensate for this inaccuracy, since only the provided reference signal content is filtered. In addition, mitigation of the mirror-frequency interference due to the I/Q imbalance is also properly handled in the proposed structure.

However, the proposed algorithm still has some limitations. First, purely digital mitigation can only be performed, if the distortion-producing signals are also received at the BB, i.e., only distortions by the interferers inside the A/D conversion band can be handled. Distortions created by the interferers out of the digitized bandwidth cannot be reproduced. The low RF selectivity typical for SDRs makes that even more difficult. This limitation has been solved in [11] by integrating an RF nonlinearity model into the RF front-end. In this case, all possible distortions that appear at the full receiver RF bandwidth are included, and only those falling into the desired BB are further processed in the digital domain. However, this solution requires considerable amount of additional hardware to be implemented on chip. An alternative would be to use an ADC with a higher sampling rate or parallel A/D interfaces, each digitizing a subset of the total receiver bandwidth. It is likely that ADCs with higher sampling rates will be feasible in the future due to fast-growing technology for digital circuits. On the other hand, purely digital mitigation has significant benefits. As desired and reference signals are obtained from a single A/D chain, both signals are perfectly aligned and the additional mismatch reported in [11] does not occur. Moreover, very flexible implementation of the algorithm on an FPGA or digital signal processor can be achieved without employing additional hardware. Thereby, runtime reconfigurability of filter characteristics, step sizes, and other parameters of the algorithm is realizable and perfectly meets the SDR concept.

Second, in-band distortions on top of the main distortion-producing signals at the BB, which are considered in the mitigation structure, cause an error for the distortion estimates, and thus reduce the mitigation performance. However, it has been found that the limitations set by these distortions can be alleviated by increasing the AF lengths. The same applies in the case of memory effects in receivers. In general, longer AFs can compensate mismatches between the real hardware and the simplified mitigation model to a certain extent. However, using a model that mimics the real situation as closely as possible is essential as has been shown in this paper.

Third, the achievable mitigation performance depends on the filter characteristics of the band-splitting stage, as discussed in Subsection III-A. In order to provide a clean reference signal for the nonlinearity modeling and AF stages, the filters need to have sufficient stopband attenuation. Moreover, filter characteristics are application-specific and depend on actual center frequency and bandwidth of the desired and blocker signals at hand. If the channel allocation is known to be static, re-tuning of the filters can be done based on simple energy detector decisions about strong signals currently being present. In case of dynamic carrier allocation with varying center frequencies and bandwidths, e.g., for multicarrier signals, the correct filter cut-off frequencies can be defined via FFT. This is the typical scenario considered for CRs [2], [4], [7].

In Section IV, the efficiency of the nonlinearity mitigation algorithm is successfully verified in AWGN channels through simulations and RF measurements with cable connections. In addition, the performance is verified with more realistic high-PAPR signals in frequency-selective channel conditions in Subsection IV-D. The mitigation architecture stays essentially the same if the input signal level is varying due to a realistic radio channel with fading phenomena. The optimal coefficients for the AFs depend solely on the receiver hardware and its nonlinear behavior. Therefore, the optimal AF coefficients do not depend on input signal or channel variations. However, in practice, the adaptation of the AF coefficients is affected by the input signal power level variations, e.g., due to the channel fading. If the signal is in the linear region of the receiver, it is challenging to obtain the AF coefficients for the receiver nonlinearity. Other extreme case is when the signal is strongly saturating or clipping and the AF coefficient adaption is interfered because the nonlinearity model does not take into account the very strong nonlinear behavior. In [34], it has been shown through extensive system-level simulations for RF nonlinearities that this kind of nonlinearity mitigation algorithm can be applied even under demanding frequency-selective and fast-fading channels while providing a considerable mitigation performance. Other important conclusion is that it is beneficial to bypass the nonlinearity mitigation algorithm when the signal-to-interference ratio is already high without the mitigation [13], [34]. This way power consumption is reduced and it is also guaranteed that the nonlinearity mitigation algorithm does not limit the overall performance.

VI. Conclusions

In this paper, a novel approach for modeling the RF and BB distortions created in wideband DCR chain has been presented. Compared to prior work, a more complete model has been developed, taking into account the most significant distortions created by a DCR. This allows for cleaning the entire BB signal from nonlinear distortions and mirror-frequency interference. The design of a digital feed-forward mitigation algorithm, that incorporates the cascaded BB model, has been addressed in detail. Simulation results with the two-tone and BPSK-modulated signals were presented to show the effectiveness of this approach that provides a significant performance improvement over previous solutions. Moreover, the RF and BB distortions in real-world RF measurements have been successfully mitigated, hence proving that both types of nonlinear distortions really co-exist and confirming applicability of the proposed mitigation architecture in practice. Finally, significant enhancement in the linearity of the front-end has been achieved, allowing for simple and low-cost receiver architectures for SDR and CR. Furthermore, the presented algorithm is generally applicable for wideband DCRs and is not restricted to the SDR. Our future work will address, e.g., methods to relax the burden on the A/D interface, through alternative analog or hybrid analog-digital reference generation methods combined with reference ADC.

Acknowledgment

M. Grimm would like to thank Prof. Mikko Valkama and the administration of the International Graduate School on Mobile Communications that made his three-month research stay at Tampere University of Technology, Finland, possible.

References

[1] B. Razavi, “Design considerations for direct-conversion receivers,” *IEEE Trans. Circuits Syst. II*, vol. 44, no. 6, pp. 428–435, June 1997.

[2] ——, “Cognitive radio design challenges and techniques,” *IEEE J. Solid-State Circuits*, vol. 45, no. 8, pp. 1542–1553, Aug. 2010.

[3] E. Biglieri, S. Barberis, and M. Catena, “Analysis and compensation of nonlinearities in digital transmission systems,” *IEEE J. Sel. Areas Commun.*, vol. 6, no. 1, pp. 42–51, Jan. 1988.

[4] E. Axell, G. Leus, E. G. Larsson, and H. V. Poor, “Spectrum sensing for cognitive radio : State-of-the-art and recent advances,” *IEEE Signal Process. Mag.*, vol. 29, no. 3, pp. 101–116, May 2012.

[5] J. Verlant-Chenet, J. Renard, J.-M. Dricot, P. De Doncker, and F. Horlin, “Sensitivity of spectrum sensing techniques to RF impairments,” in *Proc. IEEE 71st Vehicular Technology Conf. (VTC 2010-Spring)*, Taipei, Taiwan, May 2010, pp. 1–5.

[6] A. Zahedi-Ghasabeh, A. Tarighat, and B. Daneshrad, “Cyclo-stationary sensing of OFDM waveforms in the presence of receiver RF impairments,” in *Proc. IEEE Wireless Communications and Networking Conf. (WCNC2010)*, Sydney, Australia, Apr. 2010, pp. 1–6.

[7] M. Grimm, R. K. Sharma, M. Hein, and R. Thomä, “DSP-based mitigation of RF front-end non-linearity in cognitive wideband receivers,” *FREQUENZ Journal of RF-Engineering and Telecommunications, Special Issue WSR2012*, vol. 66, no. 9-10, pp. 303–310, Sept. 2012.

[8] D. H. Mahrof, E. A. M. Klumperink, J. C. Haartsen, and B. Nauta, “On the effect of spectral location of interferers on linearity requirements for wideband cognitive radio receivers,” in *Proc. IEEE Symp. on New Frontiers in Dynamic Spectrum (DySPAN2010)*, Singapore, Apr. 2010, pp. 1–9.

[9] M. Valkama, A. Shahed hagh ghadam, L. Anttila, and M. Renfors, “Advanced digital signal processing techniques for compensation of nonlinear distortion in wideband multicarrier radio receivers,” *IEEE Trans. Microw. Theory Tech.*, vol. 54, no. 6, pp. 2356 –2366, June 2006.

[10] A. Shahed hagh ghadam, “Contributions to analysis and DSP-based mitigation of nonlinear distortion in radio transceivers,” Ph.D. dissertation, Dept. Commun. Eng., Tampere University of Technology, Tampere, Finland, 2011.

[11] E. Keehr and A. Hajimiri, “Equalization of third-order intermodulation products in wideband direct conversion receivers,” *IEEE J. Solid-State Circuits*, vol. 43, no. 12, pp. 2853–2867, Dec. 2008.

[12] Q. Zou, M. Mikhemar, and A. H. Sayed, “Digital compensation of cross-modulation distortion in software-defined radios,” *IEEE J. Sel. Topics Signal Process.*, vol. 3, pp. 348–361, June 2009.

[13] M. Allén, J. Marttila, and M. Valkama, “Modeling and mitigation of nonlinear distortion in wideband A/D converters for cognitive radio receivers,” *European Microwave Assoc. Int. J. Microwave and Wireless Technologies*, vol. 2, no. 02, pp. 183–192, Apr. 2010.

[14] M. Grimm, R. K. Sharma, M. Hein, R. S. Thomä, and R. Zemmari, “Improved BER performance in GSM by mitigating non-linear distortions in the receiver,” in *Proc. European Microwave Conf. (EuMC)*, Nuremberg, Germany, Oct. 2013.

[15] F. Schlembach, M. Grimm, and R. Thomä, “Real-time implementation of a DSP-based algorithm on USRP for mitigating non-linear distortions in the receiver RF front-end,” in *Proc. 10th Int. Symp. on Wireless Communication Systems (ISWCS2013)*, Ilmenau, Germany, Aug. 2013.

[16] H.-H. Chen, P.-C. Huang, C.-K. Wen, and J.-T. Chen, “Adaptive compensation of even-order distortion in direct conversion receivers,” in *Proc. IEEE 58th Vehicular Technology Conf. (VTC 2003-Fall)*, vol. 1, Orlando, FL, Oct. 2003, pp. 271–274.

[17] E. Rebeiz, A. Shahed hagh ghadam, M. Valkama, and D. Cabric, “Suppressing RF front-end nonlinearities in wideband spectrum sensing,” in *Proc. 8th Int. Conf. Cognitive Radio Oriented Wireless Networks (CROWNCOM2013)*, Washington D.C., July 2013, pp. 87–92.

[18] *Universal Software Radio Peripheral*, Ettus Research LLC. [Online]. Available: http://www.ettus.com/

[19] A. A. Abidi, “Direct-conversion radio transceivers for digital communications,” *IEEE J. Solid-State Circuits*, vol. 30, no. 12, pp. 1399–1410, Dec. 1995.

[20] A. B. Carlson, P. B. Crilly, and J. C. Rutledge, *Communication Systems: An Introduction to Signals and Noise in Electrical Communication*, 4th ed. New York: McGraw-Hill, 2001, pp. 143–147.

[21] D. R. Morgan, Z. Ma, J. Kim, M. G. Zierdt, and J. Pastalan, “A generalized memory polynomial model for digital predistortion of RF power amplifiers,” *IEEE Trans. Signal Process.*, vol. 54, no. 10, pp. 3852–3860, Oct. 2006.

[22] S. C. Blaakmeer, E. A. M. Klumperink, D. M. W. Leenaerts, and B. Nauta, “Wideband balun-LNA with simultaneous output balancing, noise-canceling and distortion-canceling,” *IEEE J. Solid-State Circuits*, vol. 43, no. 6, pp. 1341–1350, June 2008.

[23] K. Kivekäs, A. Pärssinen, and K. A. I. Halonen, “Characterization of IIP2 and DC-offsets in transconductance mixers,” *IEEE Trans. Circuits Syst. II*, vol. 48, no. 11, pp. 1028–1038, Nov. 2001.

[24] P. B. Kenington, *High-Linearity RF Amplifier Design*. Norwood, MA: Artech House, 2000, pp. 74–77.

[25] L. Anttila, M. Valkama, and M. Renfors, “Circularity-based I/Q imbalance compensation in wideband direct-conversion receivers,” *IEEE Trans. Veh. Technol.*, vol. 57, no. 4, pp. 2099–2113, July 2008.

[26] L. Anttila, “Digital front-end signal processing with widely-linear signal models in radio devices,” Ph.D. dissertation, Dept. Commun. Eng., Tampere University of Technology, Tampere, Finland, 2011.

[27] J. L. Karki, “Designing for low distortion with high-speed op amps,” *Texas Instruments Analog Applicat. J.*, pp. 25–33, July 2001. [Online]. Available: http://www.ti.com/lit/an/slyt133/slyt133.pdf

[28] S. Haykin, *Adaptive Filter Theory*, 4th ed. Upper Saddle river, NJ: Prentice Hall, 2002, pp. 231–341.

[29] T. Adali, H. Li, and R. Aloysius, “On properties of the widely linear MSE filter and its LMS implementation,” in *Proc. 43rd Annu. Conf. Information Sciences and Systems (CISS2009)*, Baltimore, MD, Mar. 2009, pp. 876–881.

[30] H. Ku and J. S. Kenney, “Behavioral modeling of nonlinear RF power amplifiers considering memory effects,” *IEEE Trans. Microw. Theory Tech.*, vol. 51, no. 12, pp. 2495–2504, Dec. 2003.

[31] F. G. A. Neto, V. H. Nascimento, and M. T. M. Silva, “Reduced-complexity widely linear adaptive estimation,” in *Proc. 7th Int. Symp. Wireless Communication Systems (ISWCS2010)*, York, United Kingdom, Sept. 2010, pp. 399–403.

[32] R. Meyer, R. Reng, and K. Schwarz, “Convolution algorithms on DSP processors,” in *Int. Conf. Acoustics, Speech, and Signal Process.*, vol. 3, Toronto, Canada, Apr. 1991, pp. 2193–2196.

[33] T. B. Sørensen, P. E. Mogensen, and F. Frederiksen, “Extension of the ITU channel models for wideband (OFDM) systems,” in *Proc. IEEE 62nd Vehicular Technology Conf. (VTC 2005-Fall)*, vol. 1, Dallas, TX, Sept. 2005, pp. 392–396.

[34] D. Dupleich, M. Grimm, F. Schlembach, and R. S. Thomä, “Practical aspects of a digital feedforward approach for mitigating non-linear distortions in receivers,” in *Proc. 11th Int. Conf. Telecommunications in Modern Satellite, Cable and Broadcasting Services (TELSIKS2013)*, Niš, Serbia, Oct. 2013, pp. 170–177.

Michael Grimm was born in Weimar, Germany, on January 7th, 1986. He received the Dipl.-Ing. degree in electrical engineering and information technology from Ilmenau University of Technology, Germany, in 2009.

He is currently with the Electronic Measurement Research Lab within the International Graduate School on Mobile Communications at Ilmenau University of Technology as a Researcher working towards the Dr.-Ing. degree (Ph.D.). His research interests include software defined and cognitive radio, RF impairment mitigation, mixed-signal circuit design, and FPGA-based embedded signal processing.

Markus Allén (S'10) was born in Ypäjä, Finland, on October 28, 1985. He received the B.Sc. and M.Sc. degrees in signal processing and communications engineering from Tampere University of Technology, Finland, in 2008 and 2010, respectively.

He is currently with the Department of Electronics and Communications Engineering at Tampere University of Technology as a Researcher heading towards the Ph.D. degree. His current research interests include cognitive radios, analog-to-digital converters, receiver front-end nonlinearities and their digital mitigation algorithms.

Jaakko Marttila (S'10) was born in Tampere, Finland, on March 30, 1982. He received the M.Sc. degree in signal processing and communications engineering from Tampere University of Technology (TUT), Tampere, Finland, in 2010.

He is currently working towards the Ph.D. degree at TUT, Department of Electronics and Communications Engineering as a Researcher. At present, his main research topic is quadrature sigma-delta analog-to-digital (AD) conversion. Generally, his research interests include AD techniques for software defined and cognitive radios, and related interference mitigation algorithms.

Mikko Valkama (S'00, M'02) was born in Pirkkala, Finland, on November 27, 1975. He received the M.Sc. and Ph.D. degrees (both with honours) in electrical engineering (EE) from Tampere University of Technology (TUT), Finland, in 2000 and 2001, respectively. In 2002 he received the Best Ph.D. Thesis award by the Finnish Academy of Science and Letters for his dissertation entitled "Advanced I/Q signal processing for wideband receivers: Models and algorithms".

In 2003, he was working as a visiting researcher with the Communications Systems and Signal Processing Institute at SDSU, San Diego, CA. Currently, he is a Full Professor and Department Vice Head at the Department of Electronics and Communications Engineering at TUT, Finland. He has been involved in organizing conferences, like the IEEE SPAWC'07 (Publications Chair) held in Helsinki, Finland. His general research interests include communications signal processing, estimation and detection techniques, signal processing algorithms for software defined flexible radios, cognitive radio, digital transmission techniques such as different variants of multicarrier modulation methods and OFDM, radio localization methods, and radio resource management for ad-hoc and mobile networks.

Reiner Thomä (M'92–SM'99–F'07) received the Dipl.-Ing. (M.S.E.E.), Dr.-Ing. (Ph.D.E.E.), and the Dr.-Ing. habil. degrees in electrical engineering and information technology from Technische Hochschule Ilmenau, Germany, in 1975, 1983, and 1989, respectively.

From 1975 to 1988, he was a Research Associate in the fields of electronic circuits, measurement engineering, and digital signal processing at the same university. From 1988 to 1990, he was a Research Engineer at the Akademie der Wissenschaften der DDR (Zentrum für Wissenschaftlichen Gerätebau). During this period he was working in the field of radio surveillance. In 1991, he spent a three-month sabbatical leave at the University of Erlangen-Nürnberg (Lehrstuhl für Nachrichtentechnik). Since 1992, he has been a Professor of electrical engineering (electronic measurement) at TU Ilmenau where he was the Director of the Institute of Communications and Measurement Engineering from 1999 until 2005. With his group, he has contributed to several European and German research projects and clusters such as WINNER, PULSERS, EUWB, NEWCOM, COST 273, 2100, IC 1004, EASY-A, EASY-C. Currently he is the speaker of the German nation-wide DFG-focus project UKoLOS, Ultra-Wideband Radio Technologies for Communications, Localization and Sensor Applications (SPP 1202). His research interests include measurement and digital signal processing methods (correlation and spectral analysis, system identification, sensor arrays, compressive sensing, time-frequency and cyclostationary signal analysis), their application in mobile radio and radar systems (multidimensional channel sounding, propagation measurement and parameter estimation, MIMO-, mm-wave-, and ultra-wideband radar), measurement-based performance evaluation of MIMO transmission systems including over-the-air testing in virtual electromagnetic environments, and UWB sensor systems for object detection, tracking and imaging.

Prof. Thomä is a member of URSI (Comm. A), VDE/ITG. Since 1999 he has been serving as chair of the IEEE-IM TC-13 on Measurement in Wireless and Telecommunications. In 2007 he was awarded IEEE Fellow Member and received the Thuringian State Research Award for Applied Research both for contributions to high-resolution multidimensional channel sounding.